



National Library
of Canada

Bibliothèque nationale
du Canada

Canadian Theses Service

Service des thèses canadiennes

Ottawa, Canada
K1A 0N4

NOTICE

The quality of this microform is heavily dependent upon the quality of the original thesis submitted for microfilming. Every effort has been made to ensure the highest quality of reproduction possible.

If pages are missing, contact the university which granted the degree.

Some pages may have indistinct print especially if the original pages were typed with a poor typewriter ribbon or if the university sent us an inferior photocopy.

Previously copyrighted materials (journal articles, published tests, etc.) are not filmed.

Reproduction in full or in part of this microform is governed by the Canadian Copyright Act, R.S.C. 1970, c. C-30.

AVIS

La qualité de cette microforme dépend grandement de la qualité de la thèse soumise au microfilmage. Nous avons tout fait pour assurer une qualité supérieure de reproduction.

S'il manque des pages, veuillez communiquer avec l'université qui a conféré le grade.

La qualité d'impression de certaines pages peut laisser à désirer, surtout si les pages originales ont été dactylographiées à l'aide d'un ruban usé ou si l'université nous a fait parvenir une photocopie de qualité inférieure.

Les documents qui font déjà l'objet d'un droit d'auteur (articles de revue, tests publiés, etc.) ne sont pas microfilmés.

La reproduction, même partielle, de cette microforme est soumise à la Loi canadienne sur le droit d'auteur, SRC 1970, c. C-30.

THE UNIVERSITY OF ALBERTA

A DIAGNOSTIC MODEL FOR MIXING HEIGHTS APPLICABLE TO
NOCTURNAL RADIATION INVERSIONS

by

PANAGIOTIS KLIVOKIOTIS

A THESIS

SUBMITTED TO THE FACULTY OF GRADUATE STUDIES AND RESEARCH
IN PARTIAL FULFILMENT OF THE REQUIREMENTS FOR THE DEGREE
OF MASTER OF SCIENCE

IN

METEOROLOGY

DEPARTMENT OF GEOGRAPHY

EDMONTON, ALBERTA

FALL, 1988

Permission has been granted to the National Library of Canada to microfilm this thesis and to lend or sell copies of the film.

The author (copyright owner) has reserved other publication rights, and neither the thesis nor extensive extracts from it may be printed or otherwise reproduced without his/her written permission.

L'autorisation a été accordée à la Bibliothèque nationale du Canada de microfilmer cette thèse et de prêter ou de vendre des exemplaires du film.

L'auteur (titulaire du droit d'auteur) se réserve les autres droits de publication; ni la thèse ni de longs extraits de celle-ci ne doivent être imprimés ou autrement reproduits sans son autorisation écrite.

ISBN 0-315-45673-6

THE UNIVERSITY OF ALBERTA

RELEASE FORM

NAME OF AUTHOR PANAGIOTIS KLIVOKIOTIS
TITLE OF THESIS A DIAGNOSTIC MODEL FOR MIXING
HEIGHTS APPLICABLE TO NOCTURNAL
RADIATION INVERSIONS
DEGREE FOR WHICH THESIS WAS PRESENTED MASTER OF SCIENCE
YEAR THIS DEGREE GRANTED FALL, 1988

Permission is hereby granted to THE UNIVERSITY OF ALBERTA LIBRARY to reproduce single copies of this thesis and to lend or sell such copies for private, scholarly or scientific research purposes only.

The author reserves other publication rights, and neither the thesis nor extensive extracts from it may be printed or otherwise reproduced without the author's written permission.

(SIGNED) Panagiotis Klivokiotis.....

PERMANENT ADDRESS:

AFON DIDASKALOU 32.....

ALIMOS, ATHENS, GREECE.....

.....

DATED August 16, 1988

THE UNIVERSITY OF ALBERTA
FACULTY OF GRADUATE STUDIES AND RESEARCH

The undersigned certify that they have read, and recommend to the Faculty of Graduate Studies and Research, for acceptance, a thesis entitled A DIAGNOSTIC MODEL FOR MIXING HEIGHTS APPLICABLE TO NOCTURNAL RADIATION INVERSIONS submitted by PANAGIOTIS KLIVOKIOTIS in partial fulfilment of the requirements for the degree of MASTER OF SCIENCE in METEOROLOGY.

.....

Supervisor

.....

.....

Date.....

To

Christine and Nicholas,

"ΤΗΝ ΕΤΔΑΙΜΟΝΙΑΝ ΟΥΚ ΕΝ ΤΩ
ΠΟΛΛΑ ΚΕΚΤΗΣΘΑΙ ΓΙΓΝΕΣΘΑΙ,
ΑΛΛ' ΕΝ ΤΩ ΤΗ ΨΤΧΗ ΕΤ ΔΙΑ-
ΚΕΙΣΘΑΙ."

Aristotle

for they stood by me in hunger and diet till this
work to be completed. Yet they proved that happiness
may exist even where money do not.

Acknowledgments

The author would like to express his sincere appreciation to Dr. K.D. Hage for the supervision and the positive guidance in the many areas needed in this work. The author would like as well to express his deep respects to Dr. E.R. Reinelt for his encouragement and most of all for the financial support needed during the course of this work. The Institute of Earth and Planetary Physics, the University of Alberta and the Atmospheric Environment Service (Scientific Department) covered partly, by providing part-time employment, the overall financing.

Many thanks are due to the Air Pollution Control Division, Alberta Environment and specifically to Mr. R. Angle for permission to use facilities and equipment for the experimental work. The author owes special thanks to Mr. Joe Godin, technician of Alberta Environment, whose experience and good will helped to complete the experiment on schedule.

Last but not least the author thanks Dr. R.B. Charlton, Division of Meteorology, University of Alberta and Dr. D.J. Wilson, Mechanical Engineering, University of Alberta for review, corrections and challenging arguments as members of the examining committee.

Abstract

Two diagnostic models are used to estimate the time changes of mixed layer height on clear mornings after sunrise. Both begin with the nocturnal inversion temperature profile predicted by Brunt's radiational cooling with modifications by Anfossi and others. The first model is a simple practical one which assumes a dry adiabatic mixed layer. The second model utilizes Deardorff's steady-state entrainment by convection for the temperature profile in the upper portion of the mixed layer. Both models require estimates of the morning minimum temperature, the maximum temperature of the previous day, the time span between these two temperatures, the height of the top of the nocturnal inversion at the time of minimum temperature, and the surface temperature at times for which the mixing heights are calculated.

The second model also requires an estimate of the ratio of the vertical temperature gradient within the nocturnal inversion at the top of the mixed layer to the vertical temperature gradient within the upper portion of the mixed layer. The models are tested using minisonde temperature profile and supplementary observations on seven mornings. Some difficulties were encountered in the identification of both the entrainment layer and the mixed layer using minisonde data. The models fail in the presence of strong thermal advection but may be useful on mornings with clear skies and light winds. The best results are found for low

mixing/heights within the first few hours following the time
of minimum temperature.

Chapter	Table of Contents	Page
1.	INTRODUCTION	1
	1.1 Diurnal development of the boundary layer	1
	1.2 Convective boundary layer	5
	1.3 Height of the mixed layer	7
	1.4 Methods of measuring mixing heights	14
	1.5 Radiational contribution in determining the height of the mixed layer	17
	1.6 General approach	19
2.	THEORETICAL ANALYSIS AND MODELS	21
	2.1 Background	21
	2.2 Brunt's simplified radiation model	24
	2.3 Theory of the entrainment model	42
	2.3.1 Turbulent kinetic energy and the dynamic energy equations	42
	2.3.2 The mixed layer model	52
3.	Experiment	69
	3.1 Introduction	69
	3.2 Topography of the area	69
	3.3 Climatology of Edmonton	72
	3.4 Scheduling of observations. Experimental program.	74
	3.5 Observation periods	77
	3.5.1 First general observation period	77
	3.5.1.1 Summary of synoptic conditions	77
	3.5.1.2 Relevant data	77
	3.5.2 Second general observation period	82
	3.5.2.1 Summary of synoptic conditions. ...	82
	3.5.2.2 Relevant data	84

3.5.3	Third general observation period	87
3.5.3.1	Summary of synoptic conditions.	87
3.5.3.2	Relevant data	89
3.5.4	Fourth general observation period	93
3.5.4.1	Summary of synoptic conditions.	93
3.5.4.2	Relevant data	93
4.	Mixing Height models/	97
4.1	Introduction	97
4.2	Basic assumptions	98
4.3	No capping inversion-encroachment	99
4.4	General structure entrainment model: Steady state case	103
4.5	Input data and results	106
4.6	Estimation of the nocturnal inversion height and RMSE of the models.	128
5.	Summary, Conclusions and Recommendations	135
	Bibliography	142
	Appendix I	147
	Appendix II	148

List of Tables

Table	Page
2.1	Rate of change of the irradiance with respect to the temperature as a function of the temperature T28
3.1	Instruments and priority of measured quantities75
3.2	Summary of measurements and data78
3.3	Wind measurements at 10m80
3.4	Minisonde temperature data based on an assumed rate of ascent of 3m/s80
3.5	Temperature, pressure and humidity at the surface at the onset of the minisonde releases82
3.6	Wind data at 10m height84
3.7	Minisonde data based on an assumed rate of ascent 3m/s86
3.8	Surface temperature, relative humidity and pressure during the minisonde releases87
3.9	Wind measurements at 10m89
3.10	Temperature, pressure and humidity at the surface on the onset of the minisonde releases89
3.11	Minisonde temperature data based on an assumed rate of ascent of 3m/s91
3.12	Wind measurements at 10m95
3.13	Temperature, humidity and pressure at the surface during the onset of the minisonde releases.95
3.14	Minisonde temperature data based on an assumed rate of ascent 3m/s96
4.1	Input data to estimate the mixing heights118
4.2	Estimation of the nocturnal inversion height130
4.3	Estimation of the RMSE for the Encroachment model132

Table

Page

4.4	Estimation of the RMSE for the GSE-s.s. model	132
4.5	Average observed mixing heights estimated by the indicated methods	133

Table 3.3 Wind measurements at 10m

TIME(MST):	0617	0700	0745	0830	0915	1000	1045
DIRECTION:	187	189	181	191	193	213	251
SPEED :	2.3	2.9	2.1	2.6	1.7	2.3	2.4

b) Double theodolite minisonde temperature at indicated height (m), for the first approximately 4 min. of ascent are listed in Table 3.4

Table 3.4 Minisonde temperature data based on an assumed rate of ascent of 3m/s

H m	T ₀₆₁₇ °C	T ₀₇₀₀ °C	T ₀₇₄₅ °C	T ₀₈₃₀ °C	T ₀₉₁₅ °C	T ₁₀₀₀ °C	T ₁₀₄₅ °C
SFC	5.0	5.9	8.1	10.5	12.9	16.8	20.1
30	6.2	6.4	8.2	10.5	12.9	16.6	19.7
60	9.0	8.9	9.4	11.1	14.3	16.0	19.2
90	11.2	11.7	11.4	14.0	15.1	15.8	18.8
120	12.8	13.8	13.0	16.2	15.3	15.8	18.7
150	13.7	15.2	14.4	17.4	15.4	16.0	18.7
180	14.5	16.6	15.6	18.7	16.2	18.3	18.7
210	15.6	17.9	16.5	19.5	17.3	20.7	18.7
240	16.9	18.5	17.3	19.9	18.7	21.7	18.7
270	17.8	18.9	18.0	20.3	19.4	21.9	18.8
300	18.4	19.5	18.6	20.5	19.8	22.0	20.0
330	18.7	20.0	19.0	20.4	19.9	22.0	21.6
360	19.5	20.1	19.3	20.3	19.9	22.0	22.1
390	19.7	20.2	19.4	20.2	20.1	22.0	22.2
420	19.7	20.4	19.4	20.5	20.1	22.0	22.2
450	19.7	20.5	19.4	21.1	20.0	22.0	22.2
480	19.7	20.5	19.5	21.3	19.9	21.8	22.1
510	19.6	20.4	19.7	21.6	19.9	21.9	22.1
540	19.6	20.3	19.9	21.7	19.8	22.1	22.0
570	19.6	20.2	20.0	21.8	19.7	22.1	19.8
600	19.6	20.3	20.2	21.7	19.6	22.0	19.7
630	19.6	20.7	20.2	21.7	19.6	21.7	19.7
660	19.6	20.9	20.2	21.6	19.5	21.3	19.7
690	19.5	20.9	20.1	21.5	19.3	21.3	19.6

c) Table 3.5 presents measurements of standard shelter

This page has been removed
due to poor print quality

Fig. 3.7 Radiance of Stony Plain (WSE) on October 2, 1987
at 1200Z (temperature history T_H is valid at 0000Z)

temperature($^{\circ}\text{C}$), wet bulb temperature($^{\circ}\text{C}$) relative humidity(%) from Feuchte type hygrometer, station surface pressure(kpa), ventilated temperature at 8m($^{\circ}\text{C}$)

Table 3.5 Temperature, humidity and pressure at the surface at the onset of the minisonde releases

MST	Temp. $^{\circ}\text{C}$	T_w $^{\circ}\text{C}$	T_8 $^{\circ}\text{C}$	R.H. %	Pressure kpa
0617	5.0	5.2	6.4	100	93.13
0700	5.2	5.3	5.9	100	93.13
0745	6.2	6.0	8.3	96	93.12
0830	9.1	7.6	9.4	81	93.12
0915	15.4	10.3	-	43	93.12
1013	17.8	11.8	-	38	93.11
1046	19.7	12.4	20.0	34.5	-
1100	21.2	12.4	-	33	-

3.5.2 Second general observation period

Date :October 3, 1987

Sunrise (MST) :0639

Apparent noon (MST):1249

3.5.2.1 Summary of synoptic conditions.

During the second general observation period, central Alberta remained under the influence of the maritime polar air mass modified considerably during the previous 24 hours. It became warmer and drier. The circulation was dominated by a series of low pressure centers to the north and a series of high pressure centers to the south. A low pressure center was located near the border of Manitoba and the Northwest Territories west of the coast of Hudson Bay. Another low pressure center was located northwest of Great

This page has been removed
due to poor print quality

Fig. 3.8 Synoptic surface conditions on October 3, 1987 at
1200Z.

Slave Lake, in the midway from the border of the Northwest Territory and Yukon Territory. A frontal line connecting the two low centers extended south through Eastern British Columbia and through Eastern Manitoba. To the south a high pressure center was situated just west of the coast of Washington and another main high pressure center was situated over Iowa. Central Alberta was influenced by a northwesterly flow with light winds. The sky conditions in central Alberta were overcast clearing to the south. Throughout the province of Alberta convective activity was reported as a result of an approaching upper cold front (Fig. 3.8, 3.9). At the site, the experiment was initiated with less of 1/10 sky cover and ended with overcast conditions. The relative humidity decreased from 91% to 55% at the end of the second general observation period.

3.5.2.2 Relevant data

a) Table 3.6 presents information on the direction (deg from North) and speed (m/s) of the surface wind from a propellor anemometer at 10m height.

Table 3.6 Wind data at 10m height

TIME(MST):	0630	0700	0803	0837	0915	1001
DIRECTION:	212	220	149	270	090	090
SPEED:	1.3	1.2	1.3	0.4	0.1	0.4

b) Double theodolite minisonde temperatures at indicated heights (m), for the first approximately 4 min. of ascent

This page has been removed
due to poor print quality

Fig. 3.9 Radiosonde of Stony Plain (WSE) on October 3, 1987
at 1200Z (temperature history T_H is valid at 0000Z)

are listed in Table 3.7,

Table 3.7 Minisonde data based on an assumed rate of ascent of 3 m/s

H m	T _{0.815} °C	T _{0.700} °C	T _{0.803} °C	T _{0.837} °C	T _{0.915} °C	T _{1.001} °C
SFC	7.2	5.3	7.3	10.2	16.4	17.9
30	12.4	10.8	7.4	8.8	16.0	17.2
60	16.8	14.8	9.0	9.2	15.9	16.7
90	19.0	16.8	10.0	10.5	17.1	16.8
120	20.4	17.8	12.3	11.8	17.8	16.9
150	21.2	18.4	13.6	12.5	18.2	17.0
180	22.2	18.8	14.5	12.9	18.5	17.2
210	22.8	19.3	14.9	13.2	18.7	17.3
240	23.0	19.4	15.2	13.5	19.0	17.3
270	23.0	19.4	15.5	13.9	19.2	17.2
300	22.9	19.3	15.7	14.0	19.4	17.2
330	22.7	19.2	15.8	14.0	19.5	17.1
360	22.4	19.1	15.6	13.8	19.5	17.1
390	22.2	19.0	15.4	13.7	19.4	17.0
420	22.0	18.8	15.2	13.5	19.3	16.8
450	21.8	18.6	15.0	13.2	19.2	16.6
480	21.5	18.4	14.9	13.0	18.9	16.3
510	21.3	18.1	14.7	12.9	18.7	16.1
540	21.0	17.9	14.5	12.8	18.6	15.8
570	20.8	17.7	14.3	12.7	18.3	15.6
600	20.6	17.5	14.1	12.5	18.1	15.4
630	20.4	17.3	14.0	12.3	17.9	15.3
660	20.2	17.2	13.8	12.1	17.9	15.3
690	20.2	17.2	13.8	12.1	17.6	15.1

c) Table 3.8 presents measurements of standard shelter temperature (°C), wet bulb temperature (°C), relative humidity (%) from Feuchte type hygrometer, station surface pressure (kpa), ventilated temperature at 8m (°C)

Table 3.8. Surface temperature, relative humidity and pressure during the minisonde releases

MST	Td °C	T _w °C	T _a °C	R.H. %	Pressure Kpa
0615	4.2	3.2	8.1	91	93.09
0700	5.3	4.0	7.4	93	93.08
0741	5.6	4.7	-	-	-
0803	-	-	-	-	-
0824	9.8	7.5	9.8	81	93.08
0928	16.0	10.2	13.5	56	93.08
1000	17.0	11.5	14.8	54	93.06

3.5.3 Third general observation period

Date : October 6, 1987

Sunrise (MST) : 0644

Apparent noon (MST): 1248

3.5.3.1 Summary of synoptic conditions.

During the third general observation period, central Alberta was under the influence of a maritime polar air mass. The circulation was dominated by a high pressure center north of Calgary. A near stationary front was oriented from northwest to southeast across Northern Alberta (Fig. 3.10) An upper warm front was situated along a line connecting Jasper with Rocky Mountain House and extending north of Calgary. The winds remained light and the sky was half covered with cirrus and altocumulus. Nocturnal radiation had resulted in an inversion up to about 170m topped by a nearly pseudoadiabatic lapse rate (Fig. 3.11). The relative humidity decreased from 90% to

This page has been removed
due to poor print quality

Fig. 3.10 Synoptic surface conditions on October 6, 1987 at
1200Z.

47% near the end of the experimental period.

3.5.3.2 Relevant data

a) Table 3.9 presents data on the direction (deg from North) and speed (m/s) of the surface wind from a propellor anemometer at 10m height.

Table 3.9 Wind measurements at 10m

TIME(MST):	0615	0700	0746	0830	0915	1000
DIRECTION:		273	236	223	270	310
SPEED:		1.5	1.2	0.2	0.2	1.3

b) Table 3.10 contains data on standard shelter temperature ($^{\circ}\text{C}$), wet bulb temperature ($^{\circ}\text{C}$), relative humidity (%) from Feuchte type hygrometer, station surface (kpa), ventilated temperature at 8m ($^{\circ}\text{C}$)

Table 3.10 Temperature, humidity and pressure at the surface on the onset of the minisonde releases

MST	Temp. $^{\circ}\text{C}$	T_w $^{\circ}\text{C}$	T_s $^{\circ}\text{C}$	R.H. %	Pressure kpa
0615	0.7	0.4	2.3	89	94.24
0700	0.7	-0.2	1.7	63.5	94.25
0746	2.5	1.3	2.6	87	94.24
0830	5.0	2.8	4.1	75	94.26
0915	6.6	3.8	5.9	51	94.28
1000	8.1	7.8	8.1	44	94.26

c) Double theodolite minisonde temperatures at indicated heights (m), for first approximately 4min of ascent are listed in Table 3.11

This page has been removed
due to poor print quality

Fig. 3.11 Radiosonde of Stony Plain (WSE) on October 6, 1987
at 1200Z (temperature history T_H is valid at 0000Z)

listed in Table 3.11

Table 3.11 Minisonde temperature data based on an assumed rate of ascent 3 m/s

H m	T ₀₈₁₅ °C	T ₀₇₀₀ °C	T ₀₇₄₆ °C	T ₀₈₃₀ °C	T ₀₉₁₅ °C	T ₁₀₀₀ °C
SFC	8.9	2.2	2.6	4.8	8.9	8.8
30		3.4	2.9	3.8	7.3	8.2
45	9.8					
60		4.8	3.4	3.4	6.3	7.6
90	11.3	5.8	4.2	3.2	6.0	7.0
120		6.9	5.2	3.1	5.7	6.8
135	12.3					
150		7.9	5.5	3.8	5.7	6.6
180	12.4	8.3	6.1	4.4	5.7	6.4
210		8.3	6.2	4.9	5.8	6.2
225	12.2					
240		8.1	6.1	5.0	6.2	5.8
270	11.9	8.0	6.0	4.9	6.2	5.7
300		7.8	5.9	4.8	6.1	5.8
315	11.7					
330		7.7	5.8	4.6	6.0	6.2
360	11.4	7.5	5.7	4.4	5.8	6.3
390		7.3	5.6	4.2	5.6	6.1
405	11.2					
420		7.1	5.5	4.1	5.5	6.0
450	10.9	6.9	5.4	4.0	5.4	5.7
480		6.8	5.3	3.9	5.2	5.5
495	10.7					
510		6.6	5.2	3.9	4.9	5.3
540	10.4	6.6	5.1	3.9	4.6	5.4
570		6.5	5.0	3.6	4.4	5.3
585	10.2					
600		6.4	4.8	3.6	4.2	5.3
630	9.9	6.3	4.3	3.5	4.1	5.3
660		6.2	4.2	3.2	4.0	5.2
675	9.7					
690		6.1	4.2	3.2	3.8	5.1

This page has been removed
due to poor print quality

Fig. 3.12 Synoptic surface conditions on October 12, 1987 at
1200Z.

3.5.4 Fourth general observation period

Date :October 12, 1987
Sunrise (MST) :0655
Apparent noon (MST):1247

3.5.4.1 Summary of synoptic conditions.

The circulation affecting the weather of Alberta on the 12th of October was dominated by a high pressure center situated in the southeast corner of British Columbia and two low pressure centers situated east of Great Slave Lake and north of Fort Nelson, on the border between British Columbia and the Northwest Territory. Alberta was on the warm side of a maritime arctic front situated west of the Alberta-British Columbia border, in a N-S direction. The weak pressure gradient over central Alberta resulted in light winds near the surface. Most of the stations in the region reported clear sky but with up to 2 octants of high clouds over the Edmonton area (Fig. 3.10) The air mass was warm and dry. A nocturnal inversion of magnitude about 10°C was reported at Edmonton Stony Plain (WSE) 80km northwest from our observation site at 1200Z (Fig. 3.11).

3.5.4.2 Relevant data

a) Table 3.12 contains information on the direction (deg from North) and speed (m/s) of the surface wind from a propellor anemometer at 10m height.

This page has been removed
due to poor print quality

Fig. 3.13 Radiosonde of Stony Plain (WSE) on October 12,
1987 at 1200Z (temperature history T_H is valid at 0000Z)

Table 3.12 Wind measurements at 10m.

TIME(MST):	0616	0700	0746	0830	0915	1000
DIRECTION:	180	184	186	208	0915	1000
SPEED:	2.1	2.1	1.8	1.1	1.1	3.1

*These values are 5-min averages.

b) Table 3.13 presents data of the standard shelter temperature($^{\circ}\text{C}$), wet bulb temperature($^{\circ}\text{C}$), relative humidity(%) from a Feuchte type hygrometer, station surface pressure(kpa), ventilated temperature at 8m($^{\circ}\text{C}$).

Table 3.13 Temperature, humidity and pressure at the surface on the onset of the minisonde releases.

MST	Td $^{\circ}\text{C}$	Tw $^{\circ}\text{C}$	T ₈ $^{\circ}\text{C}$	R.H. %	Pressure Kpa
0615	1.5	-0.7	1.3	88.0	92.48
0700	1.1	-0.6	1.9	84.5	92.39
0745	1.5	-0.3	1.5	86.0	92.35
0830	5.3	2.5	14.3	71.0	92.29
0915	7.8	4.4	17.4	47.0	92.24
1000	13.8	7.0	11.7	42.0	92.21

c) Single theodolite minisonde temperatures at indicated heights (m) for first approximately 4 min of ascent are listed in Table 3.14

Table 3.14 Minisonde temperature data based on an assumed rate of ascent 3 m/s.

H m	T _{0.830} °C	T _{0.700} °C	T _{0.746} °C	T _{0.853} °C	T _{0.915} °C	T _{1.001} °C
SFC	0.4	1.0	1.6	5.7	8.7	13.1
30	3.4	3.6	3.5	4.2	7.4	11.7
60	6.5	7.0	7.1	4.5	7.2	11.0
90	9.8	9.6	10.3	6.8	10.3	10.9
120	12.5	11.7	12.4	10.0	13.3	12.4
150	14.2	13.9	14.2	12.1	15.1	15.0
180	15.2	15.0	15.0	13.5	15.8	15.5
210	16.1	16.1	15.1	14.1	16.0	15.7
240	17.0	17.1	15.4	14.2	16.0	16.1
270	17.9	18.2	16.1	14.3	16.2	16.3
300	18.4	18.9	17.4	14.2	16.7	16.3
330	18.5	19.1	17.9	15.1	16.8	16.4
360	18.6	19.2	18.0	15.3	16.8	16.2
390	18.6	19.6	18.7	15.5	16.8	16.0
420	19.0	20.0	19.0	15.8	16.8	16.0
450	19.2	20.0	18.9	15.9	16.8	16.2
480	19.3	19.9	18.7	15.9	16.8	16.1
510	19.2	19.7	18.5	15.4	16.8	16.0
540	19.0	19.4	18.3	15.3	16.8	16.0
570	18.7	19.2	18.1	15.4	16.5	16.0
600	18.5	19.0	18.1	15.4	16.4	16.0
630	18.3	18.9	17.9	15.1	16.5	16.0
660	18.0	18.8	17.8	15.0	16.5	16.0
690	17.7	18.6	17.6	14.5	16.6	16.0

4. Mixing-Height models

4.1 Introduction

A simple analytical diagnostic formula for the height of the mixed layer as it develops on clear mornings over land in response to solar heating is desired.

The basic assumptions are:

1. A radiational nocturnal inversion has developed at the surface under all circumstances justifying the validity of the Anfossi equation presented in Section 2.2
2. The development of the convective turbulent mixed layer follows the principles and assumptions described by the models presented in Section 2. Idealized temperature profiles under stable and unstable conditions or before and after sunrise are illustrated in Fig. 4.1

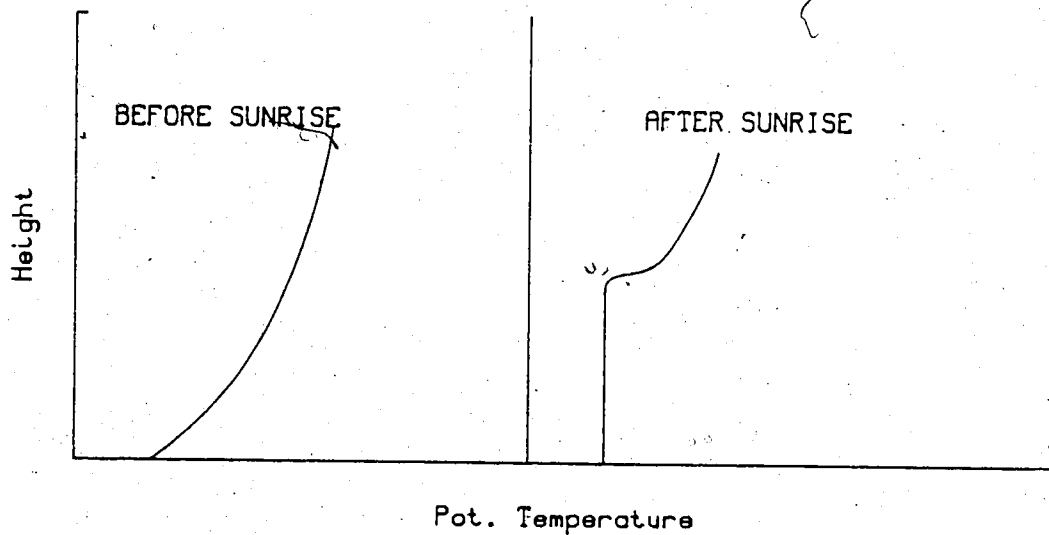


Fig. 4.1 Two ideal temperature profiles before and after sunrise.

4.2 Basic assumptions

1. Following Anfossi, et al (1976) the atmosphere is assumed to be a medium with lower and upper boundaries, the last being variable with time and identified by the condition $\frac{\partial T}{\partial z}=0$.
2. The short wave radiation is assumed unaffected as it passes through the atmosphere. As a result, the effect of the solar radiation is reflected only by the surface temperature.
3. Calm conditions or light winds of speed no more than 15km/hr at approximately 100-150m, are assumed for the validity of the simple solution, in order to avoid advection effects.
4. Clear skies or thin high clouds are assumed in order to justify the use of Brunt's theory which resulted in the equation $\frac{\partial T}{\partial t}=K_R \frac{\partial T}{\partial z}$ (see Section 2.2)
5. Anfossi, et al (1976) suggest the following equation as an appropriate solution to Brunt's equation:

$$T(z,t) = T(0,0) - [T(0,0) - T(0,t)] \left\{ \exp\left[-\left(\frac{z}{h_i}\right)^2\right] - \frac{z}{h_i} \pi^{1/2} \operatorname{erfc}\left(\frac{z}{h_i}\right) + 0.278 \left(\frac{z}{h_i}\right) \right\}$$

or

$$T(z,t) = T(0,0) - [T(0,0) - T(0,t)] \left\{ \exp\left[-\left(\frac{z^2}{4K_R t}\right)\right] - \frac{z}{2\sqrt{K_R t}} \pi^{1/2} \operatorname{erfc}\left(\frac{z}{2\sqrt{K_R t}}\right) + 0.278 \left(\frac{z}{2\sqrt{K_R t}}\right) \right\} \quad (4-1)$$

For a specific height say $z_c = 100\text{m}$ and $\frac{z_c^2}{4K_R} = t_c$ we get

$$T(z_c, t) = T(0, 0) - [T(0, 0) - T(0, t)] \left\{ \exp\left(-\frac{t_c}{t}\right) - \sqrt{\left(\frac{t_c}{t}\right)} \operatorname{erfc}\left(\sqrt{\frac{t_c}{t}}\right) + 0.278 \left(\sqrt{\frac{t_c}{t}}\right) \right\} (4-1a)$$

4.3 No capping inversion-encroachment

Fig. 4.2 illustrates the potential temperature profile during the encroachment stage where z_i is the height of the mixed layer and h_i is the top of the nocturnal inversion. From (2-19a)

$$\frac{d\Delta\theta}{dt} = \left(\frac{\partial\theta}{\partial z}\right)_{z_i} \frac{dz_i}{dt} - \frac{\partial\theta_m}{\partial t}$$

In the case of encroachment $\Delta\theta=0$ and

$$\frac{dz_i}{dt} \left(\frac{\partial\theta}{\partial z}\right)_{z_i} = \frac{\partial\theta_m}{\partial t} \quad (4-2)$$

where $\left(\frac{\partial\theta}{\partial z}\right)_{z_i}$ is the lapse rate of the nocturnal stable layer derived from (2-13b) by replacing $q(z, t) = K_R \rho_a c \frac{\partial T}{\partial z}$

or

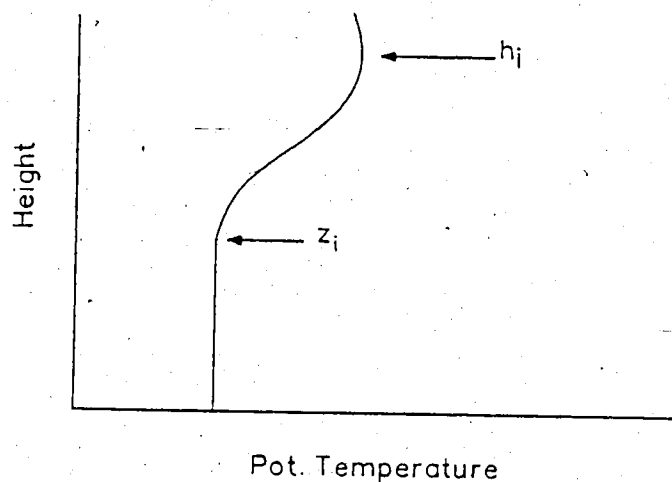


Fig. 4.2 Ideal temperature profile with no capping inversion.

$$\frac{\partial T}{\partial z} = \frac{R_N}{K_R \rho_a c_p [1 - \text{erfc}(1)]} [\text{erfc}(z/h_i) - \text{erfc}(1)] \quad (4-3)$$

or

$$\left(\frac{\partial T}{\partial z}\right)_{z_i} = C_0 \text{erfc}(z_i/h_i) - C_1$$

$$\text{where } C_0 = \frac{R_N}{K_R \rho_a c_p [1 - \text{erfc}(1)]}, \quad C_1 = \frac{R_N \text{erfc}(1)}{K_R \rho_a c_p [1 - \text{erfc}(1)]}$$

and $C_1 = C_0 \text{erfc}(1)$

By integrating (4-2) with respect to time:

$$\int_0^{z_i(t)} \left(\frac{\partial \theta}{\partial z}\right)_{z_i} \frac{dz_i}{dt} dt = \theta_m(t) - \theta_0$$

or

$$\int_0^{z_i(t)} \left(\frac{\partial \theta}{\partial z}\right)_{z_i} dz_i = \theta_m(t) - \theta_0 \quad (4-4)$$

From the relation

$$T = \theta \left(\frac{p}{p_0}\right)^{R/c_p}$$

we may derive a relation for the lapse rates

$$\frac{\partial T}{\partial z} = \frac{T}{\theta} \frac{\partial \theta}{\partial z} \frac{q}{c_p}$$

or

$$\frac{\partial \theta}{\partial z} = \frac{\theta}{T} \left(\frac{\partial T}{\partial z} + \frac{q}{c_p}\right)$$

As a first approximation $\theta \approx T$ and

$$\frac{\partial \theta}{\partial z} = \frac{\partial T}{\partial z} + \frac{q}{c_p} \quad (4-5)$$

We substitute (4-5) in (4-4):

$$\int_0^{z_i(t)} \left(\frac{\partial T}{\partial z} + \frac{q}{c_p} \right) z_i dz_i = \theta_m(t) - \theta_0 \quad (4-6)$$

We substitute (4-3) in its abbreviated form in (4-6) and

get:

$$\int_0^{z_i(t)} C_0 \operatorname{erfc}\left(\frac{z_i}{h_i}\right) dz_i - \int_0^{z_i(t)} C_1 dz_i + \frac{q}{c_p} \int_0^{z_i(t)} dz_i = \theta_m(t) - \theta_0$$

or

$$C_0 \int_0^{z_i(t)} \operatorname{erfc}\left(\frac{z_i}{h_i}\right) dz_i - C_1 z_i + \frac{q}{c_p} z_i = \theta_m(t) - \theta_0$$

or

$$C_0 \int_0^{z_i(t)} \operatorname{erfc}\left(\frac{z_i}{h_i}\right) dz_i + \left(\frac{q}{c_p} - C_1 \right) z_i = \theta_m(t) - \theta_0$$

or

$$C_0 \left\{ \int_0^\infty \operatorname{erfc}\left(\frac{z_i}{h_i}\right) dz_i - z_i(t) \int_0^\infty \operatorname{erfc}\left(\frac{z_i}{h_i}\right) dz_i \right\} + \left(\frac{q}{c_p} - C_1 \right) z_i = \theta_m(t) - \theta_0$$

or

$$C_0 \left[\int_0^\infty h_i(t) \operatorname{erfc}\left(\frac{z_i}{h_i}\right) d\left(\frac{z_i}{h_i}\right) - \frac{z_i(t)}{h_i} \int_0^\infty h_i \operatorname{erfc}\left(\frac{z_i}{h_i}\right) d\left(\frac{z_i}{h_i}\right) \right] + \left(\frac{q}{c_p} - C_1 \right) z_i(t) = \theta_m(t) - \theta_0 \quad (4-7)$$

Since $h_i = f(K_R, t)$ only, we may rewrite (4-7) as

$$C_0 h_i(t) \left[\int_0^\infty \operatorname{erfc}\left(\frac{z_i}{h_i}\right) d\left(\frac{z_i}{h_i}\right) - \frac{z_i}{h_i} \int_0^\infty \operatorname{erfc}\left(\frac{z_i}{h_i}\right) d\left(\frac{z_i}{h_i}\right) \right] + \left(\frac{q}{c_p} - C_1\right) z_i(t) = \theta_m(t) - \theta_0$$

or

$$C_0 h_i(t) \left[\left(\frac{z_i}{h_i}\right) \operatorname{erfc}\left(\frac{z_i}{h_i}\right) + \frac{1}{\sqrt{\pi}} (1 - \exp(-\frac{z_i^2}{h_i^2})) \right] + \left(\frac{q}{c_p} - C_1\right) z_i(t) = \theta_m(t) - \theta_0 \quad (4-8)$$

for $z_i=0$ $\theta_m(t) \equiv \theta_0$, $\left(\frac{z_i}{h_i}\right)=0$, $\operatorname{erfc}(0)=1$, $\exp(-\frac{z_i^2}{h_i^2})=1$

$$C_0 \equiv \frac{R_N}{K_R \rho_a c_p [1 - \operatorname{erfc}(1)]}, \quad C_1 = C_0 \operatorname{erfc}(1), \quad \delta\theta = \theta_m(t) - \theta_0,$$

$h_i = \sqrt{[4K_R(t-t_s)]}$, where t_s is the time of the previous day at which T is maximum and $z_* \equiv (z_i/h_i)$

Then (4-8) becomes:

$$C_0 h_i(t) \left[z_* \operatorname{erfc}(z_*) + \frac{1}{\sqrt{\pi}} (1 - \exp(-z_*^2)) \right] - \operatorname{erfc}(1) z_* + \frac{q}{c_p} z_i(t) = \delta\theta$$

or

$$\frac{C_0}{\sqrt{\pi}} [1 - \exp(-z_*^2) + z_* \sqrt{\pi} \operatorname{erfc}(z_*)] - \sqrt{\pi} \operatorname{erfc}(1) z_* = \frac{\delta\theta}{h_i} \quad (4-9a)$$

but, according to Anfossi et al (1976) $\frac{C_0}{\sqrt{\pi}} h_i(t_{\min}) = T_{\max} - T_{\min} = \Delta T$

and (4-9a) becomes

$$\frac{\Delta T}{h_i(t)} [\exp(-z_*^2) - \sqrt{\pi} z_* \operatorname{erfc}(z_*) - 1 + 0.278 z_*] + \frac{q}{c_p} z_* = \theta_0$$

or

$$0.0098 z_* - \Delta T [\exp(-z_*^2) - 1.7725 z_* \operatorname{erfc}(z_*) + 0.278 z_* - 1] = \theta_0 \quad (4-9b)$$

In our case $h_i(t)$ is considered constant beyond the time at which the temperature is minimum. Therefore $h_i(t) = h_0$ at $\theta_0 = T_{\min}$.

To allow h_i to increase with time beyond t_{\min} we should also allow ΔT to increase with time by allowing T_{\min} to continue decreasing with time. This could lead to nonpractical assumptions. Therefore $h_i(t) = h_i(0)$ is estimated from a temperature profile at T_{\min} .

The program "encroachment" computes the mixing height z_i .

4.4 General structure entrainment model: Steady state case

In this model developed by Deardorff (1979) an entrainment layer is considered (Fig. 4.3). We distinguish three basic layers described by three different processes

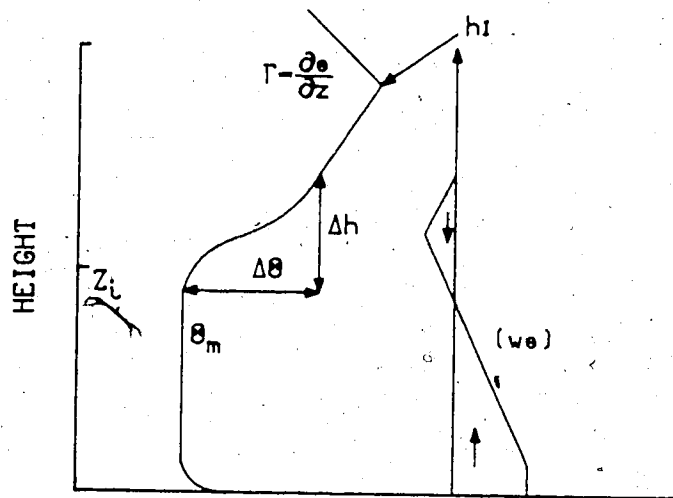


Fig. 4.3 Potential temperature and heat flux vs. height for the General Structure Entrainment model.

and consequently by three different equations.

1. Well mixed layer: Θ_m : constant

$$\frac{d\Theta_m}{dt} = \frac{1}{z_0} (w \overline{\Theta})_s \quad (4-10a)$$

2. Steady state entrainment layer:

Deardorff(1979) suggests for the steady state entrainment layer, $\Delta\Theta$: constant and $0.85 < G < 0.98$ for meaningful results.

For the steady state case

$$\frac{\Delta h}{z_0} = \frac{1-G}{G+Y-1} \quad (4-10b)$$

3. Stable Layer:

$$\left(\frac{\partial T}{\partial z}\right)_{z_0+\Delta h} = C_0 \operatorname{erfc}\left(\frac{z_0+\Delta h}{h_i}\right) - C_1$$

or from (4-5)

$$\Gamma_3 = \left(\frac{\partial \Theta}{\partial z}\right)_{z_0+\Delta h} = C_0 \operatorname{erfc}\left(\frac{z_0+\Delta h}{h_i}\right) - C_1 + \frac{q}{c_p} \quad (4-10c)$$

From (4-10b)

$$\Delta h = \frac{1-G}{G+Y-1} z_0 \quad \text{and} \quad \frac{\Delta \Theta}{\Delta h} = \frac{\Gamma_3}{G}$$

then

$$\Theta_{z_0+\Delta h} = \Theta_m + \frac{\Gamma_3}{G} \cdot \frac{1-G}{G+Y-1} z_0 =$$

$$\Theta_m + \left\{ C_0 \operatorname{erfc}\left(\frac{z_0+\Delta h}{h_i}\right) - C_1 + \frac{q}{c_p} \right\} \frac{1-G}{G(G+Y-1)} z_0 \quad (4-10d)$$

We integrate (4-10c) and get:

$$\Theta(z_0+\Delta h, t_{\min}) = \Theta(0, t_{\min}) - \Delta T (\exp(-z_0^2) - 1.7725 z_0 \operatorname{erfc}(z_0) + 0.278 z_0 - 1) + \frac{q}{c_p} (z_0 + \Delta h)$$

By replacing $\Delta h = \frac{1-G}{G+Y-1} z_0$ and substitute $\frac{1-G}{G+Y-1} \frac{z_0}{h_i} = G_y z_0$.

and $\frac{Y}{G+Y-1} \equiv Y_G$ we get:

$$\begin{aligned} \theta(z_0 + \Delta h, t_{\min}) = & \theta(0, t_{\min}) - \Delta T [\exp(-(Y_G z_{0*})^2) \\ & - 1.7725 Y_G z_{0*} \operatorname{erfc}(Y_G z_{0*}) + 0.278 Y_G z_{0*} - 1] + \frac{q}{c_p} Y_G z_{0*} \end{aligned} \quad (4-11)$$

From (4-10d) we get:

$$\theta(z_0 + \Delta h, t) = \theta(0, t) - \Delta T + \left\{ C_0 [\operatorname{erfc}(Y_G z_{0*}) - \operatorname{erfc}(1)] + \frac{q}{c_p} \right\} \frac{G}{G} z_0(t) \quad (4-12)$$

We equate (4-11) with (4-12) by making the assumption that the rate of change of the temperature with time in the stable layer is negligible after sunrise. If

$\theta_m(0, t) - \theta(0, t_{\min}) = \delta\theta$, we finally get:

$$\begin{aligned} \delta\theta = & -\Delta T [\exp(-(Y_G z_{0*})^2) \\ & - 1.7725 (Y_G - \frac{G}{G}) z_{0*} \operatorname{erfc}(Y_G z_{0*}) + 0.278 (Y_G - \frac{G}{G}) z_{0*} - 1] + \frac{q}{c_p} (Y_G - \frac{G}{G}) z_0 \end{aligned}$$

or

$$\theta_* = 0.0098 (Y_G - \frac{G}{G}) z_{0*} - \Delta T_* [\exp(-(Y_G z_{0*})^2)$$

$$- 1.7725 (Y_G - \frac{G}{G}) z_{0*} \operatorname{erfc}(Y_G z_{0*}) + 0.278 (Y_G - \frac{G}{G}) z_{0*} - 1] \quad (4-13)$$

if we will divide both sides by h_i , the nocturnal inversion height.

The equation (4-13) is reduced to the "encroachment" equation (4-9b) for $G=1$.

The program "GSE" computes the mixing height z_0 by means of (4-13).

4.5 Input data and results

The data needed are the nocturnal inversion height h_i at the time with minimum surface temperature, the temperature difference between the maximum temperature of the previous day and the minimum temperature of the current day ΔT , the temperature difference of the current hour and the minimum temperature at the surface. This temperature difference is assumed equivalent to the potential difference, $\delta\theta = \theta_m(t) - \theta_o(t)$, where $\theta_o(t) \equiv T_{\min}$.

The time and the maximum temperature have been selected from the climatological data of the International Airport of Edmonton because they were not available on the site. The time and the minimum temperature have been selected from the experimental data collected at Ellerslie.

Table 4.1 depicts the input data. It also contains three additional cases from experiments in the rural area surrounding Edmonton and carried out by the Atmospheric Environment Service. For these three cases the maximum and minimum temperatures were selected from the monthly records of Environment Canada, for the Ellerslie weather station. The times corresponding to the above temperatures was approximated by the time available on the same days in more recent years, where it was available. Figures 4.4 to 4.14 depict the temperature profiles.

In the Ellerslie experiments the observed mixing heights were estimated for the encroachment model and the General Structure Entrainment model (steady state). Fig.

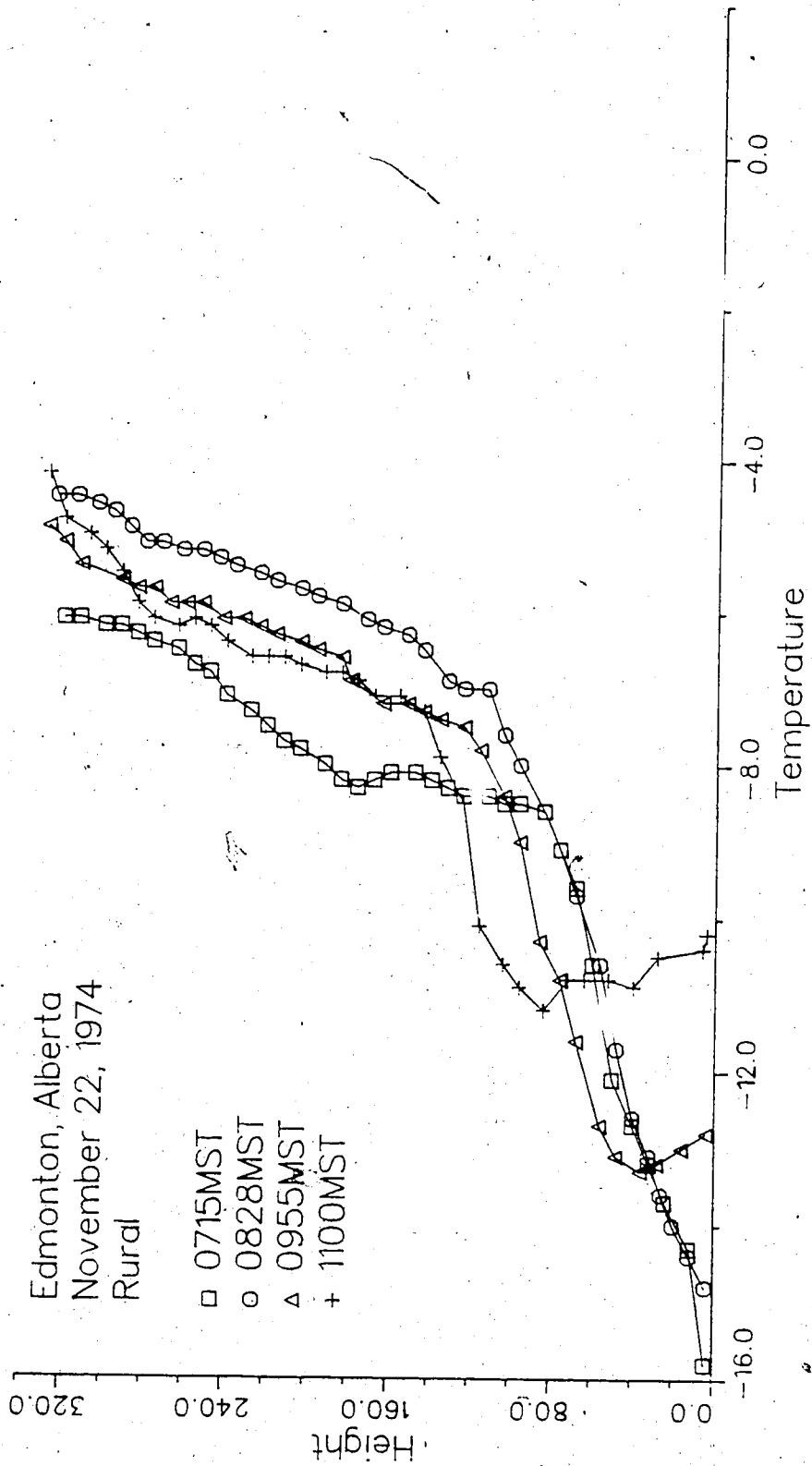


Fig. 4.4 Temperature profiles at indicated times on November 22, 1974, rural area, Edmonton, Alberta

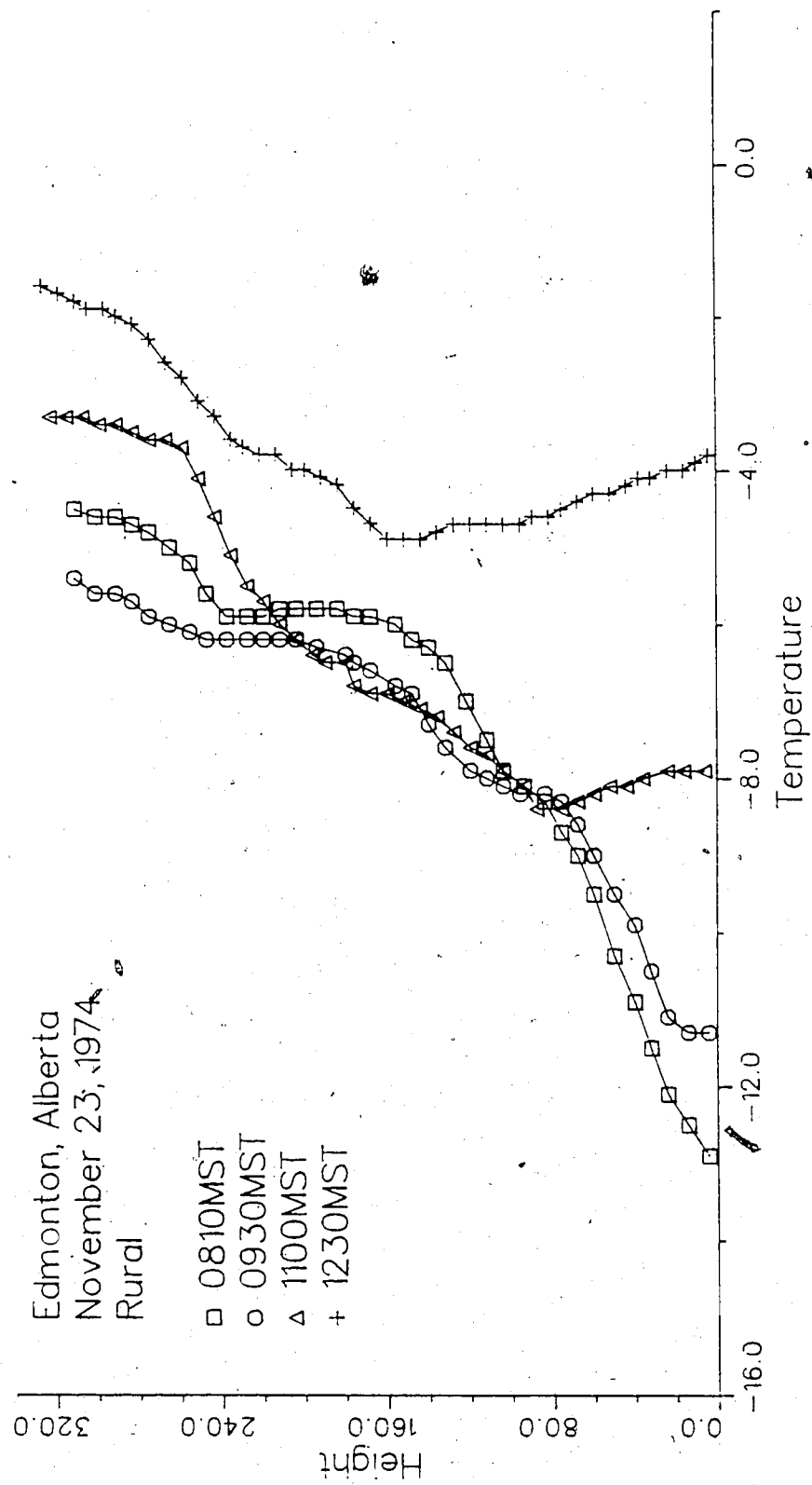


Fig. 4.5 Temperature profiles at indicated times on November 23, 1974, rural area, Edmonton, Alberta

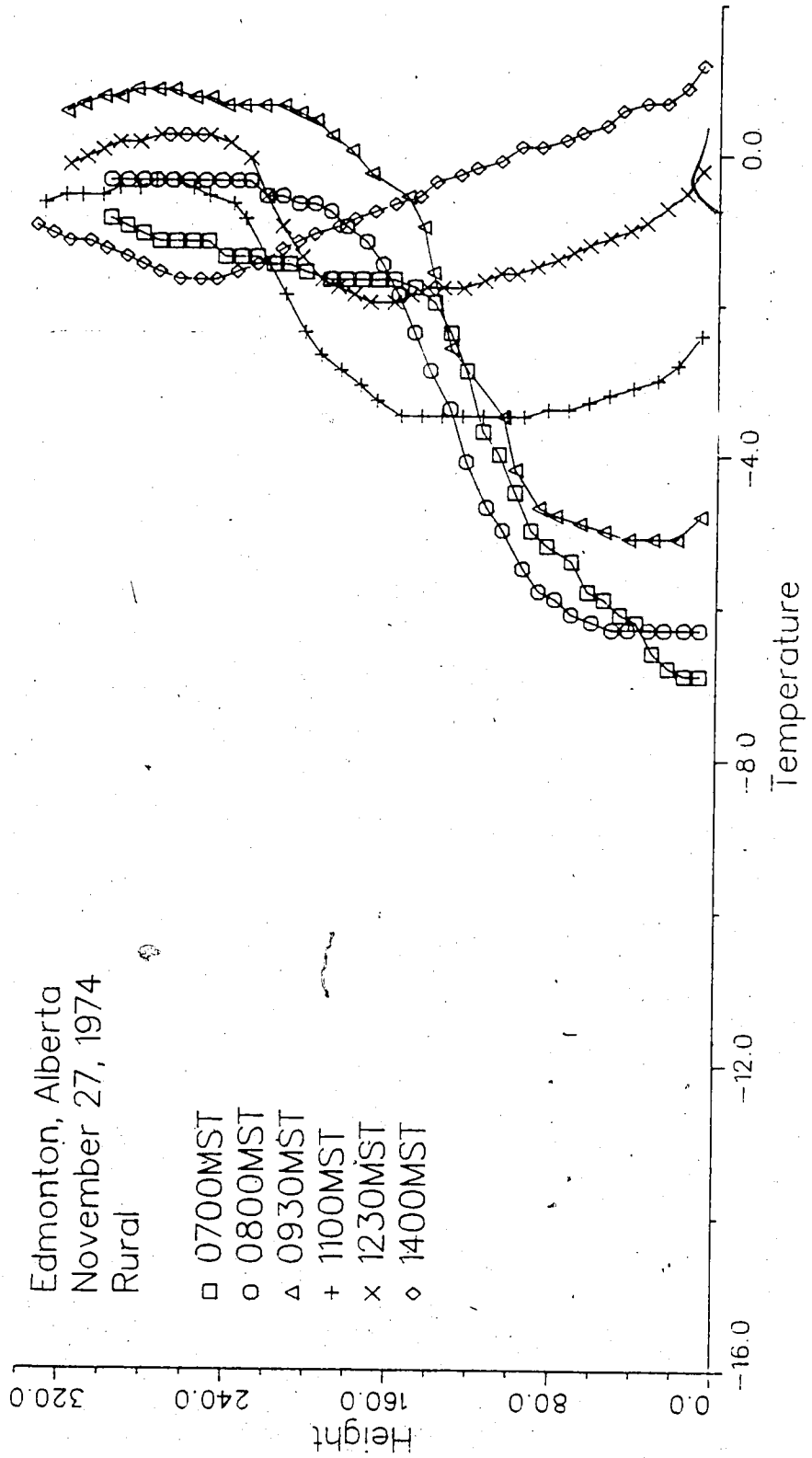


Fig. 4.6 Temperature profiles at indicated times on November 27, 1974, rural area, Edmonton, Alberta

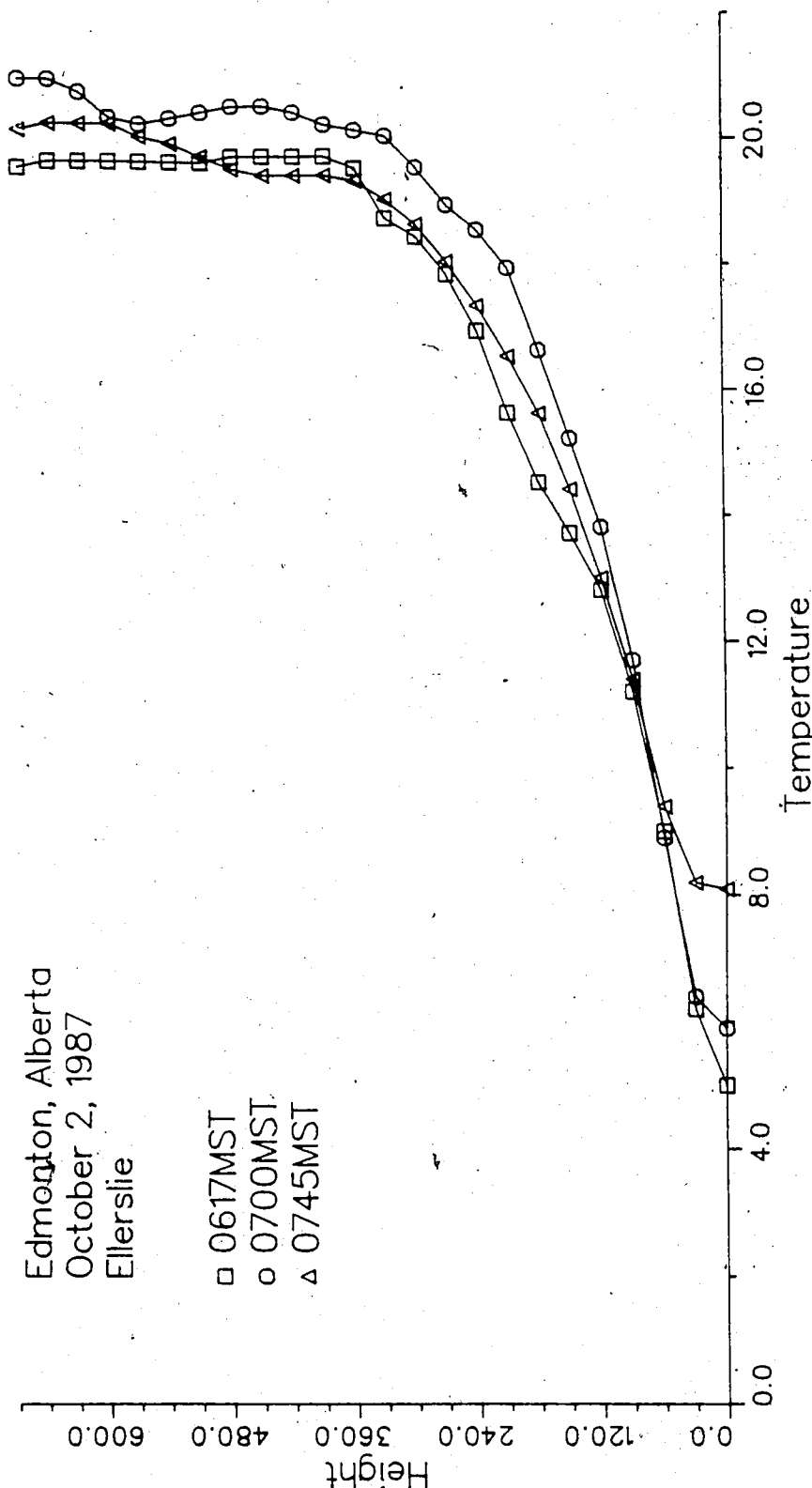


Fig. 4.7 Temperature profiles at indicated times on October 2, 1987 at Ellerslie, Edmonton, Alberta

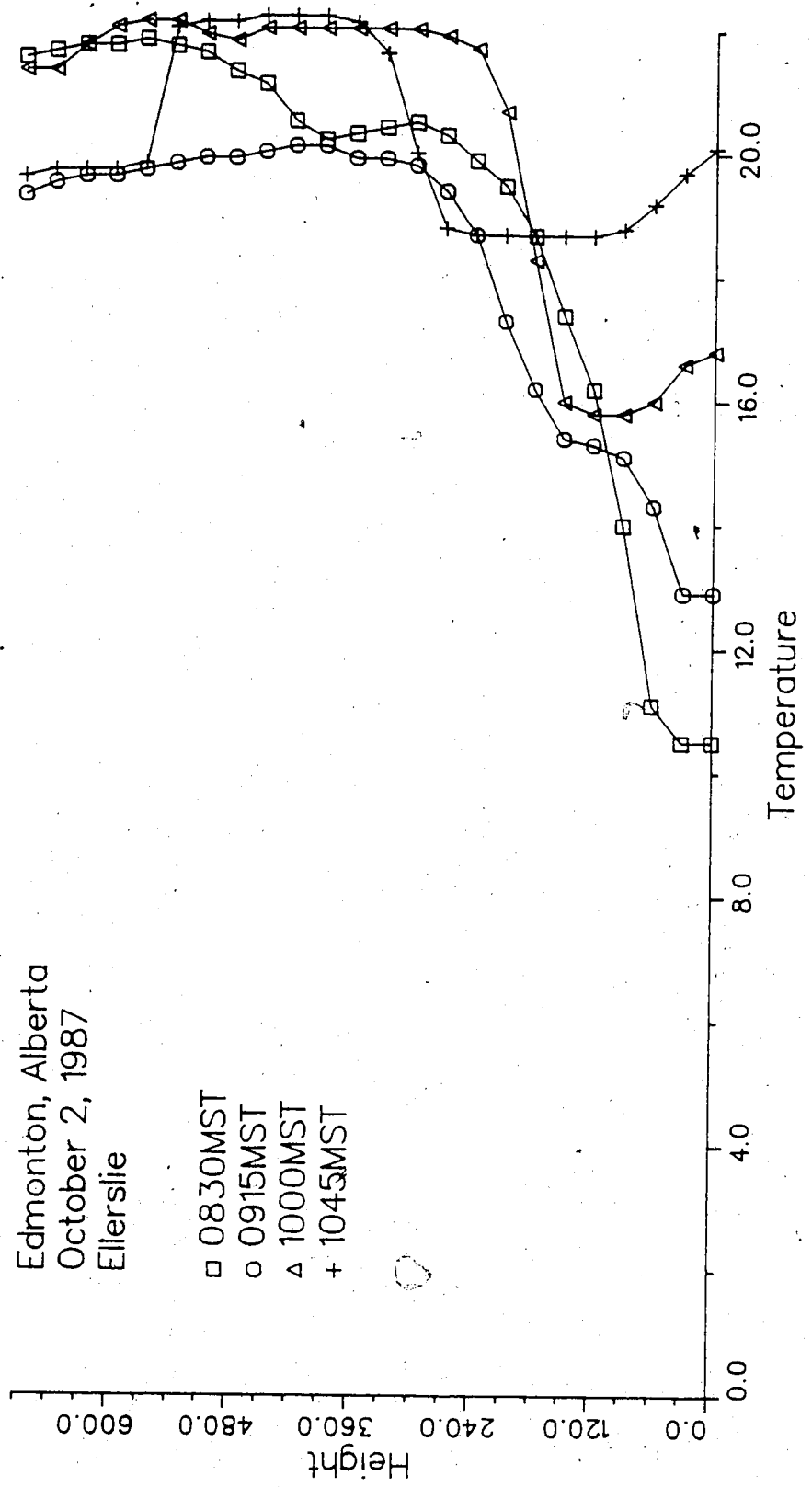


Fig. 4.8 Temperature profiles at indicated times on October 2, 1987 at Ellerslie, Edmonton, Alberta

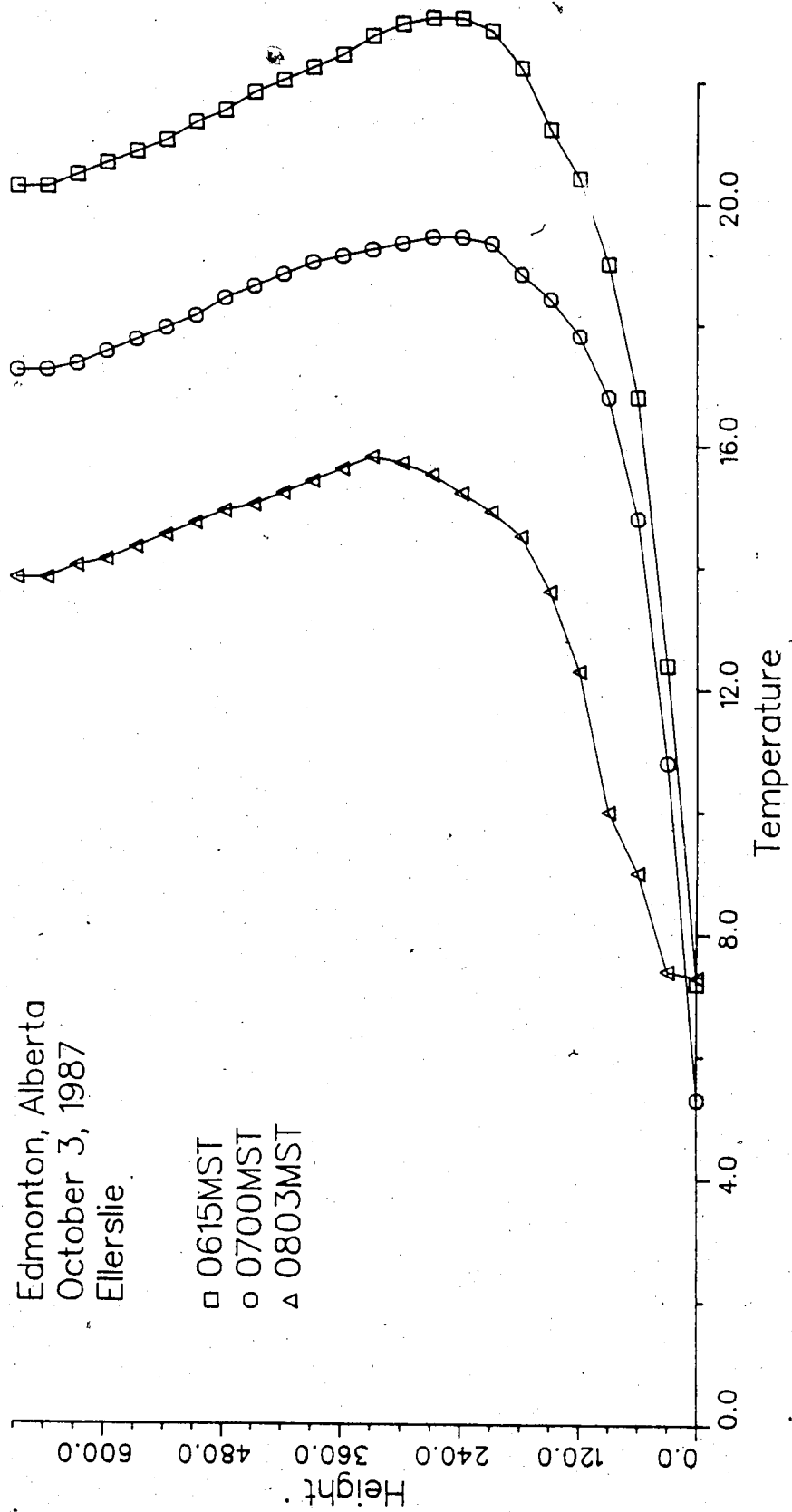


Fig. 4.9 Temperature profiles at indicated times on October 3, 1987 at Ellerslie, Edmonton; Alberta

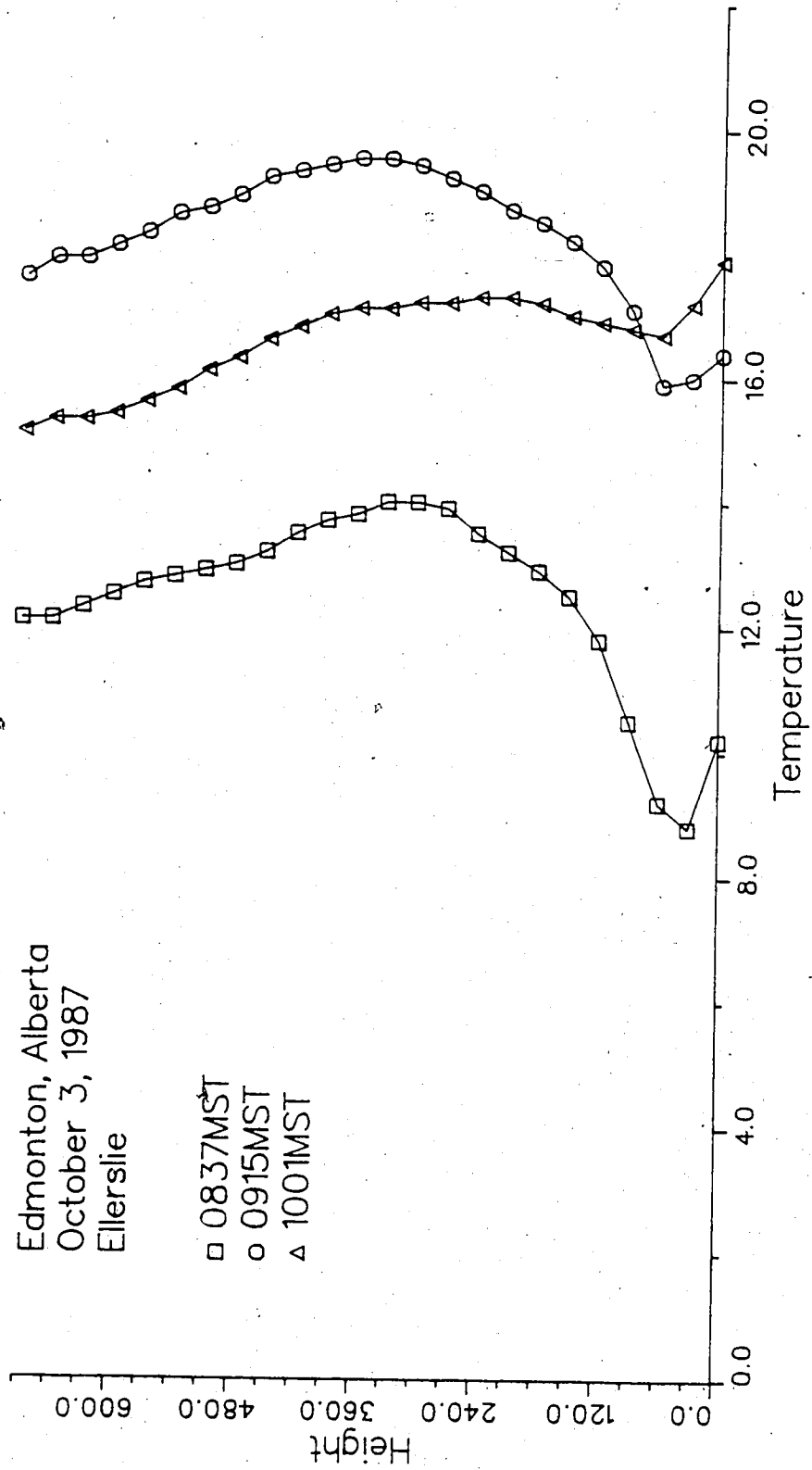


Fig. 4.10 Temperature profiles at indicated times on October 3, 1987 at Ellerslie, Edmonton, Alberta

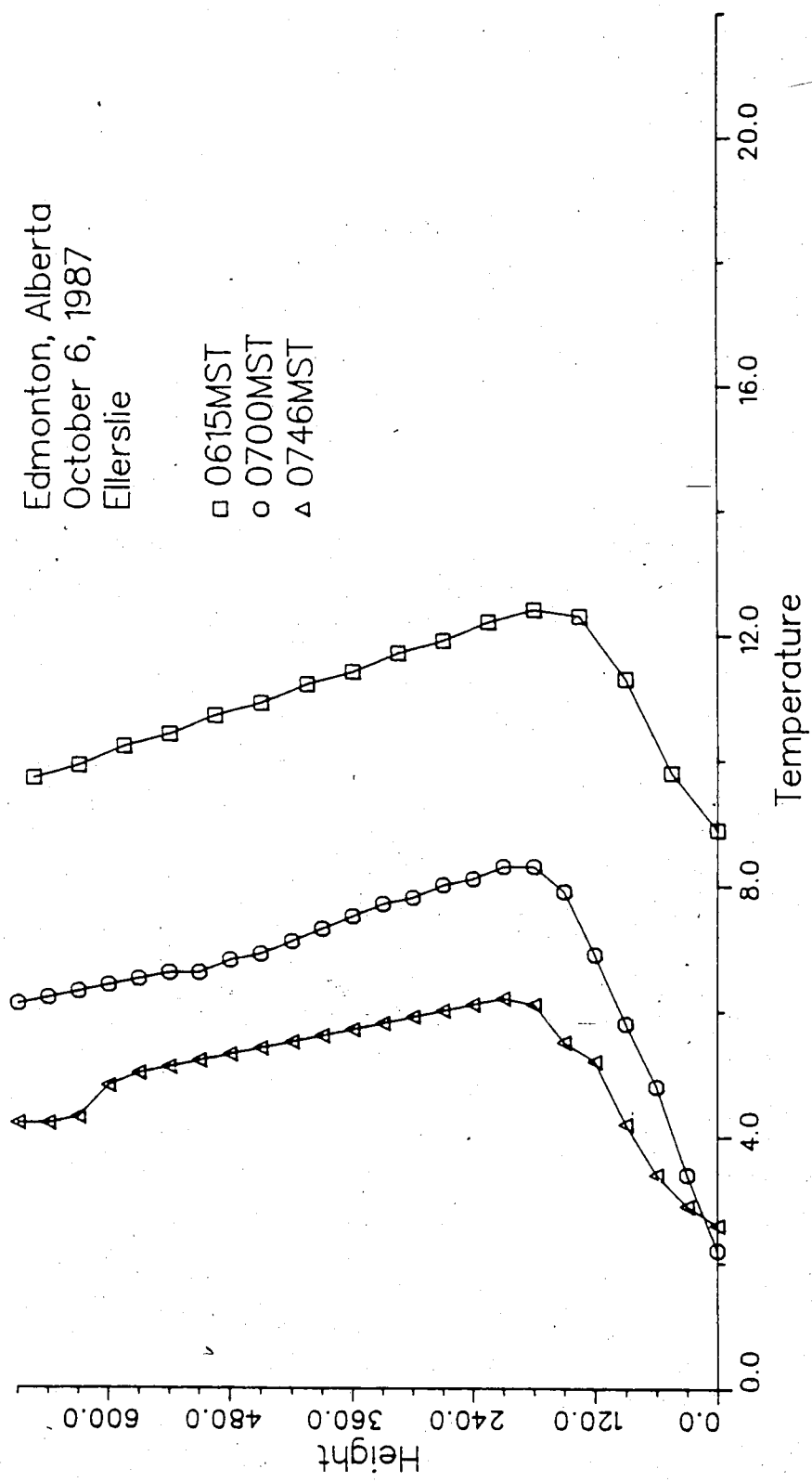


Fig. 4.11 Temperature profiles at indicated times on October 6, 1987 at Ellerslie, Edmonton, Alberta

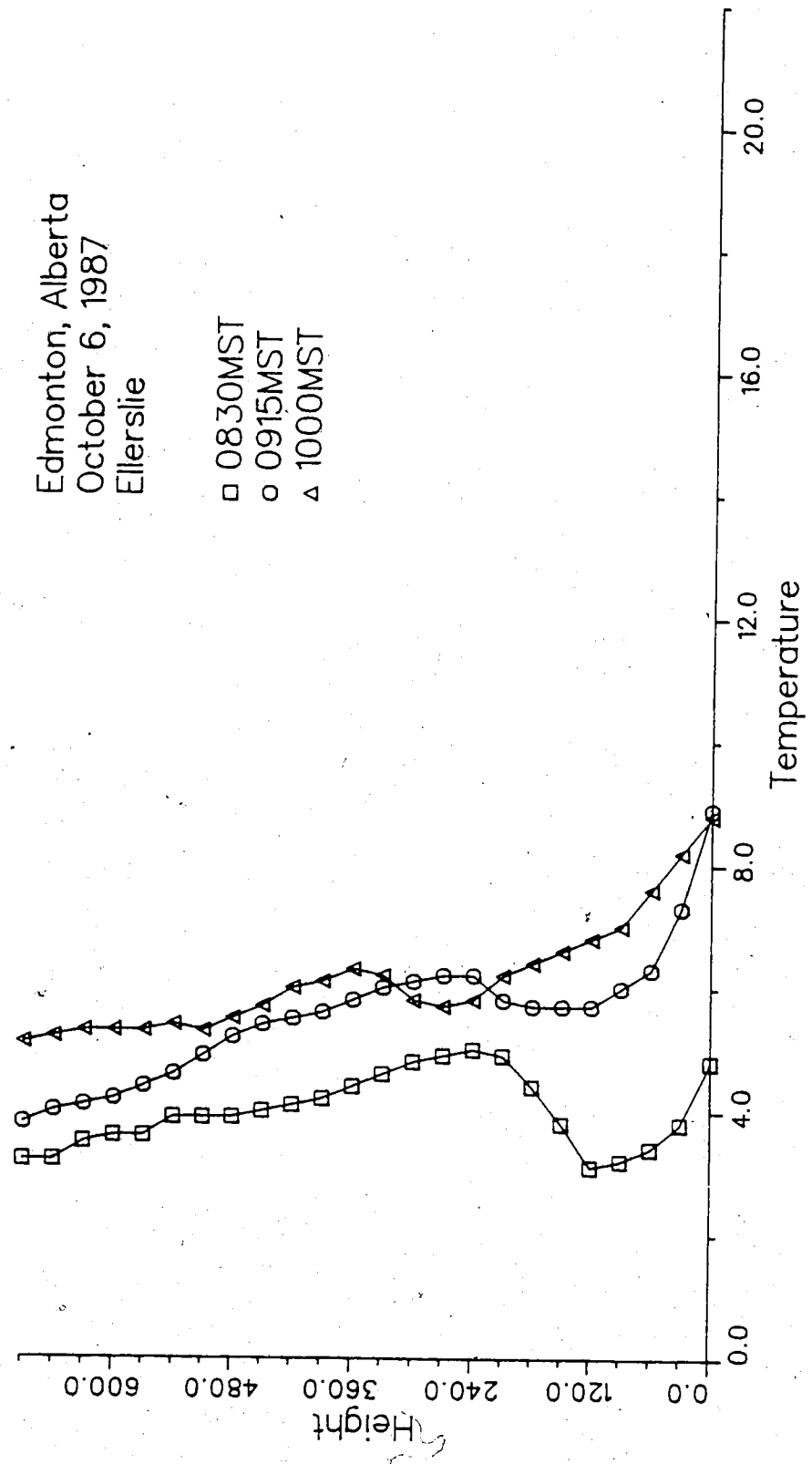


Fig. 4.12 Temperature profiles at indicated times on October 6, 1987 at Ellerslie, Edmonton, Alberta

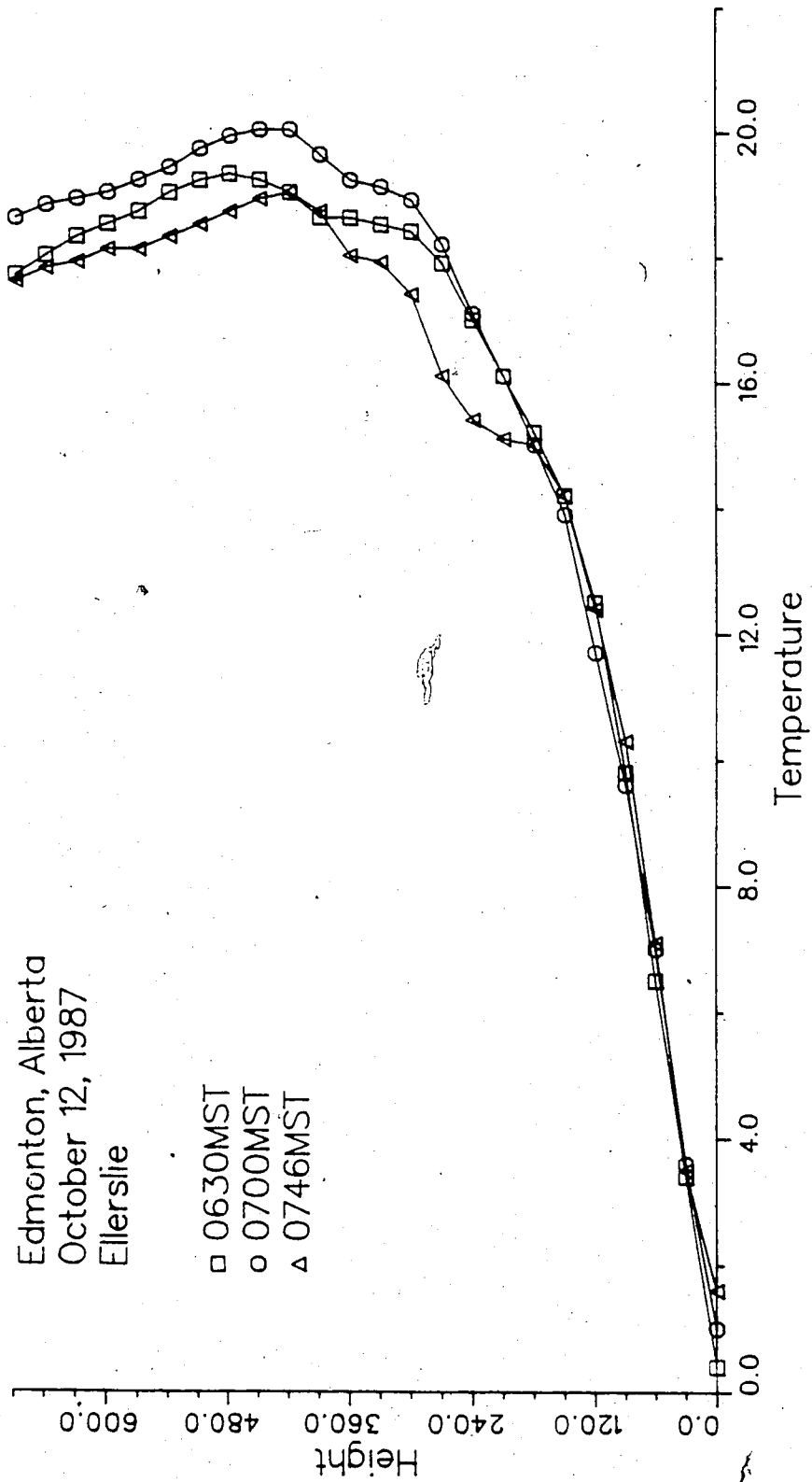


Fig. 4.13 Temperature profiles at indicated times on October 12, 1987 at Ellerslie, Edmonton, Alberta

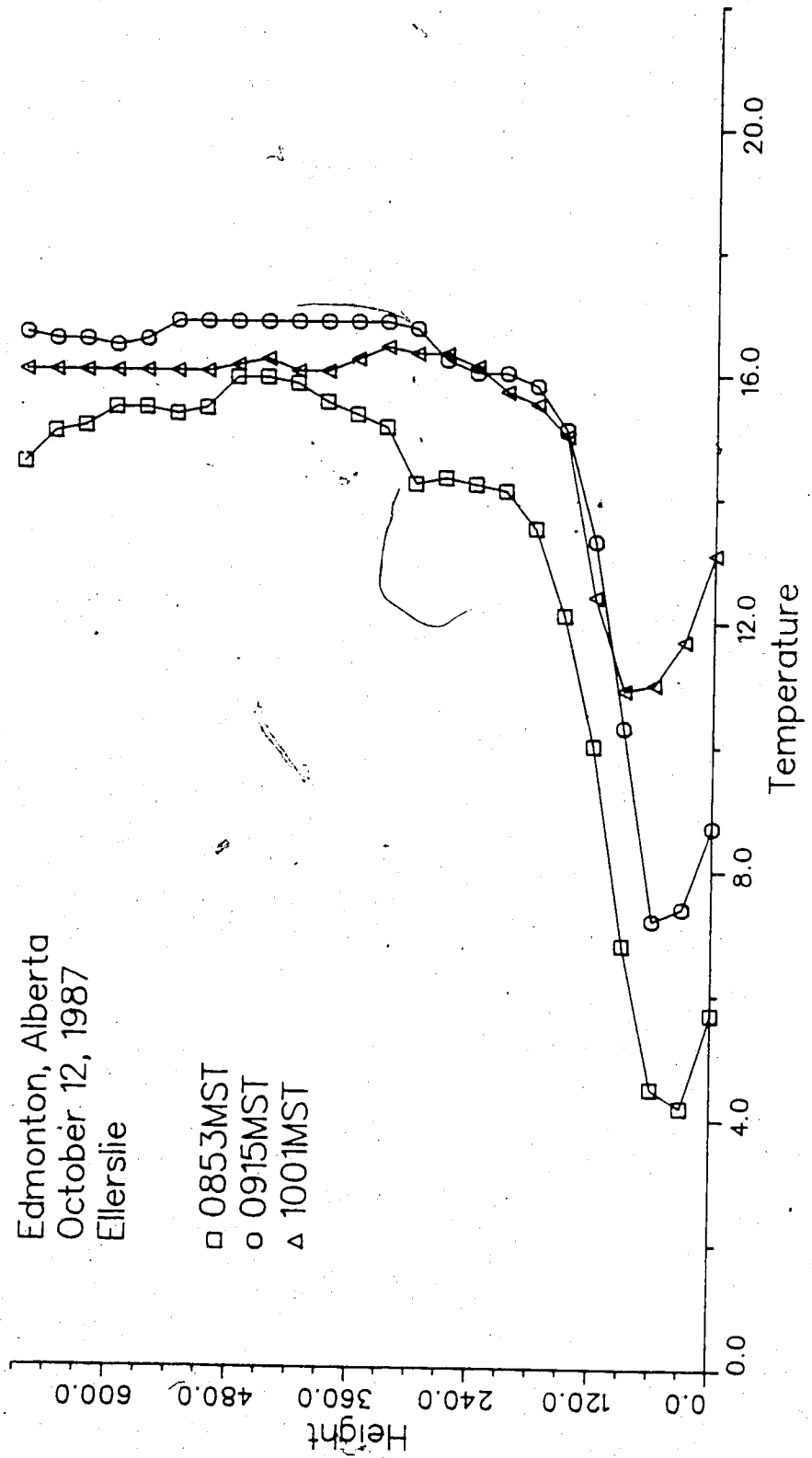


Fig. 4.14 Temperature profiles at indicated times on October 12, 1987 at Ellerslie, Edmonton, Alberta

Table 4.1 Input data to estimate the mixing heights.

Date	T_{max} °C	time MST	T_{min} °C	time MST	ΔT °C	h_i m	$\delta\theta$ at minisonde release									
							1	2	3	4	5	6				
74-11-21	-5.0	13:00														
74-11-22	-2.8	13:00	-17.8	05:00	12.8	720	2.4	3.0	5.0	7.6	14.5	14.6				
74-11-23			-14.4	06:00	11.6	291	1.6	3.1	6.5	10.6	13.6					
74-11-26	0.6	14:00	-5.6													
74-11-27	2.2		-10.0	07:00	10.6	378	3.0	3.8	5.2	7.6	9.8	11.2				
87-10-01	19.3	16:00														
87-10-02	29.1	14:00	5.9	07:00	13.4	390	0	2.2	4.6	7.0	10.9	14.2				
87-10-03	19.6	13:00	5.3	07:00	23.8	270	0	2.0	4.9	11.1	12.6					
87-10-05	17.6	16:00														
87-10-06	13.1	15:00	2.2	07:00	15.4	200	0	0.4	2.6	6.7	6.6					
87-10-11	23.4	15:00														
87-10-12	18.1	13:00	1.0	07:00	22.4	435	0	0.6	4.7	7.7	12.1					

4.15 to 4.25 depict the relation of observed and calculated mixing heights. All heights are in meters.

On November 22, 1974 the model appears to overestimate the mixing height. This overestimate increased with time. The discrepancy increased as higher mixing heights were diagnosed.

On November 23, 1974 the encroachment model demonstrated again a tendency to overestimate the observed mixing height and the discrepancy increased with time.

On November 27, 1974 the pattern followed in the two previous days appeared to change. Although the encroachment model overestimated the observed heights the discrepancy did not increase with time. The highest observed mixing height, actually seems to be underestimated.

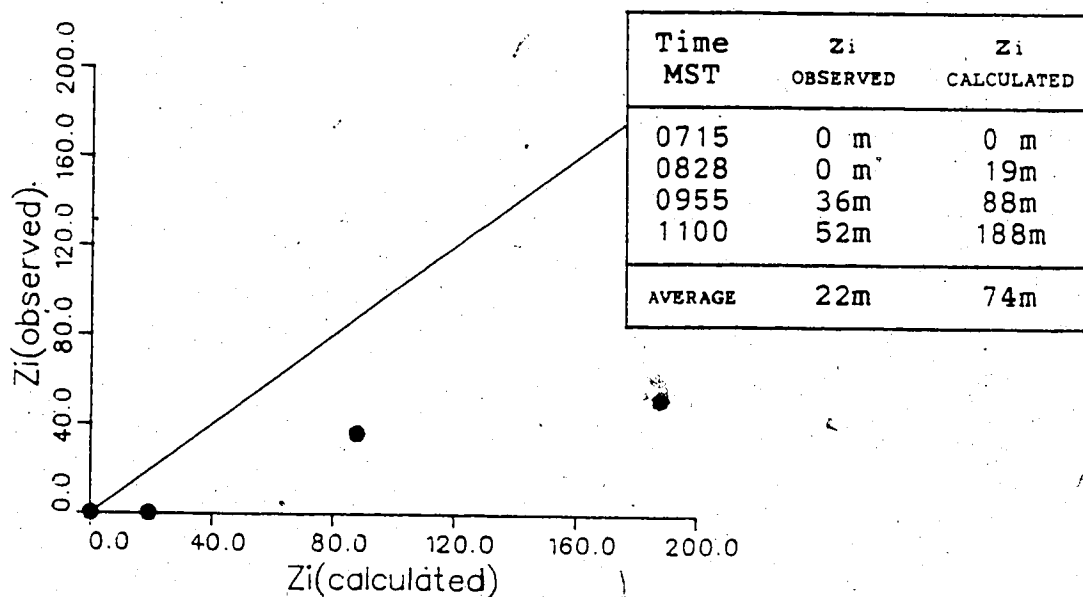


Fig. 4.15 Observed vs. calculated mixing heights with the encroachment model valid for November 22, 1974

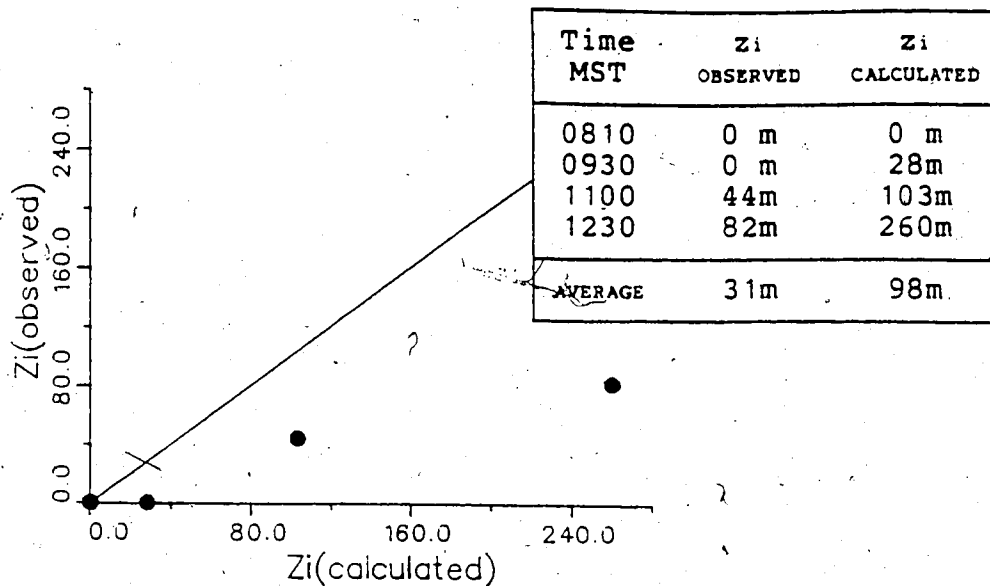


Fig. 4.16 Observed vs. calculated mixing heights with the encroachment model valid for November 23, 1974

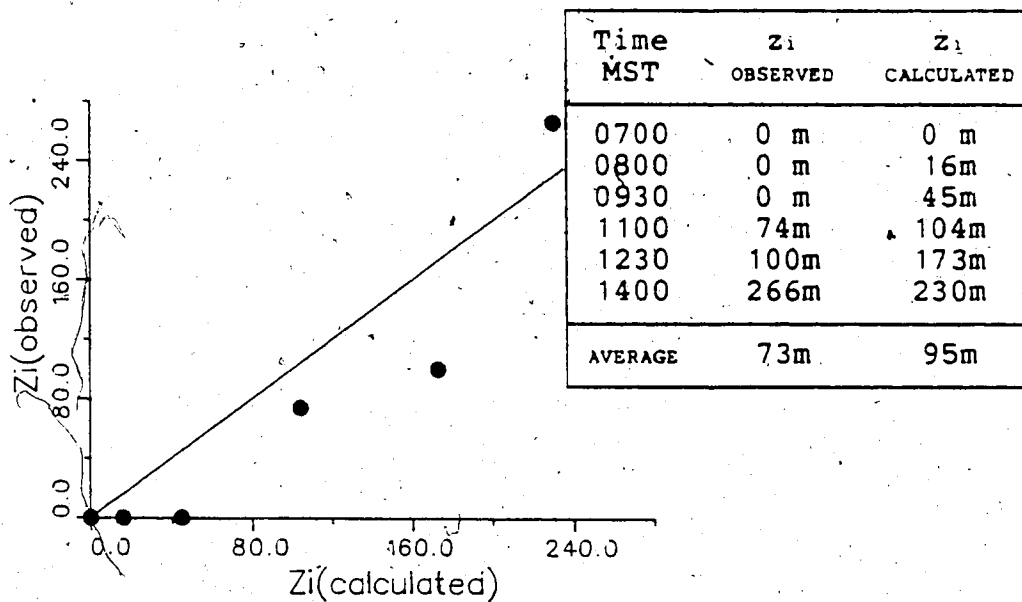


Fig. 4.17 Observed vs. calculated mixing heights with the encroachment model valid for November 27, 1974

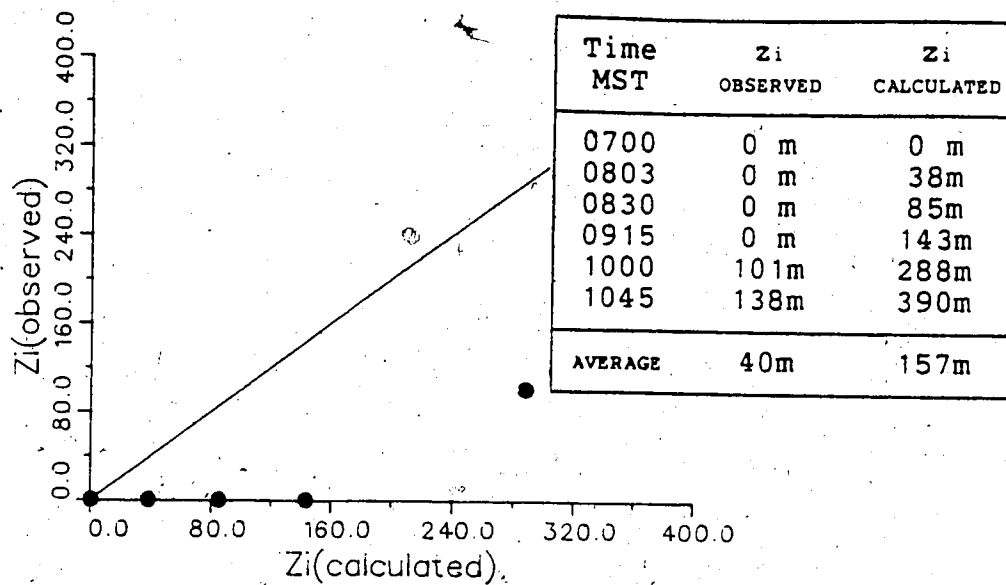


Fig. 4.18 Observed vs. calculated mixing heights with the encroachment model valid for October 2, 1987

On October 2, 1987 the encroachment model again overestimated the observed mixing height and the discrepancy increased with time.

On October 3, 1987 the model overestimated the observed mixing height. However, it appears that the pattern of increasing discrepancy was not followed. The calculated height of 38m was very close to the observed value of 35m, whereas the discrepancy decreased towards the highest observed mixing height.

October 6, 1987 the encroachment model underestimated dramatically the observed mixing heights. As Fig. 4.11 indicates, during that day a cool air advection occurred causing that abnormal behaviour of the model.

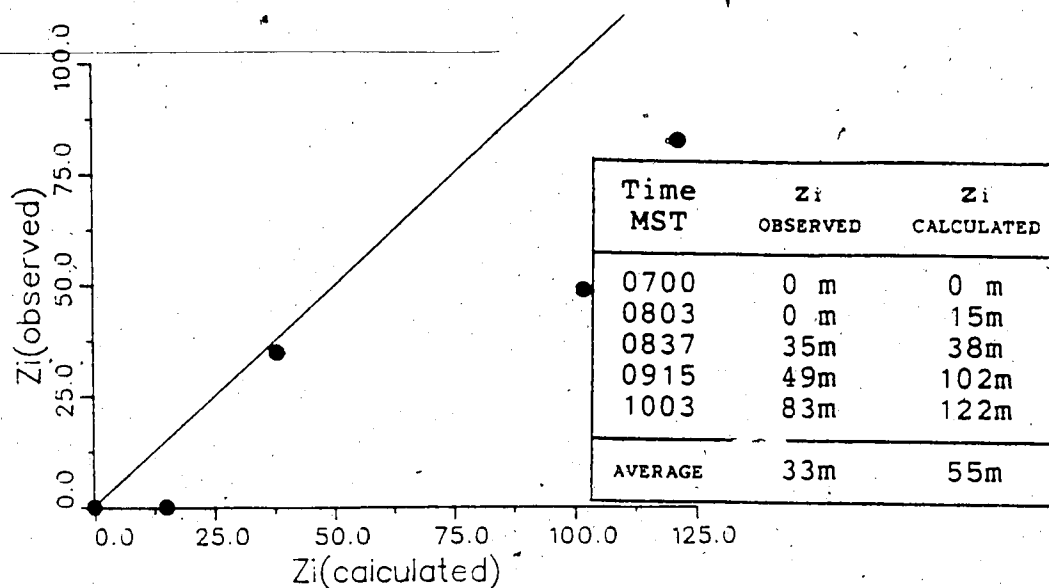


Fig. 4.19 Observed vs. calculated mixing heights with the encroachment model valid for October 3, 1987

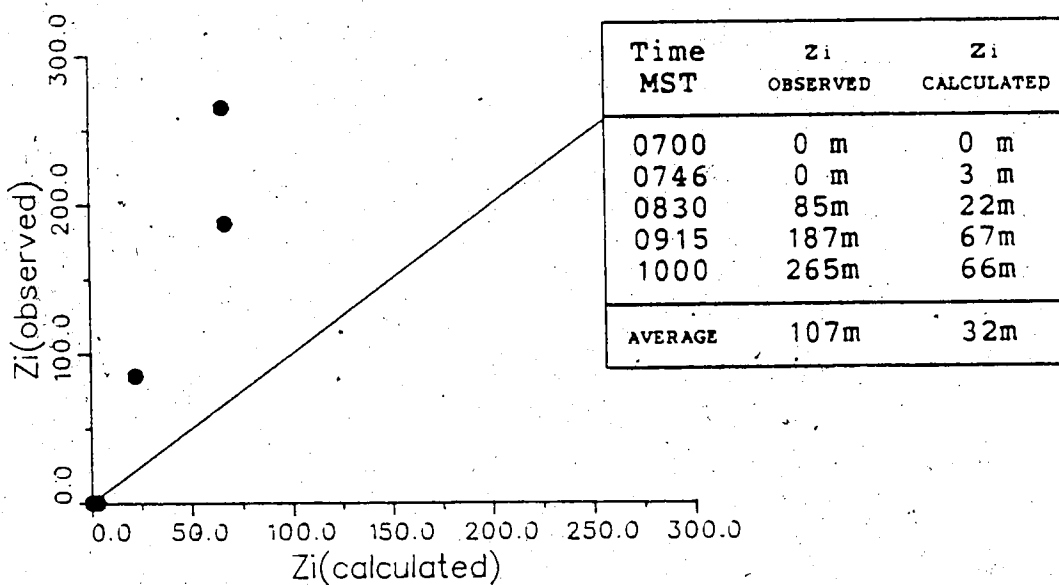


Fig. 4.20 Observed vs. calculated mixing heights with the encroachment model valid for October 6, 1987

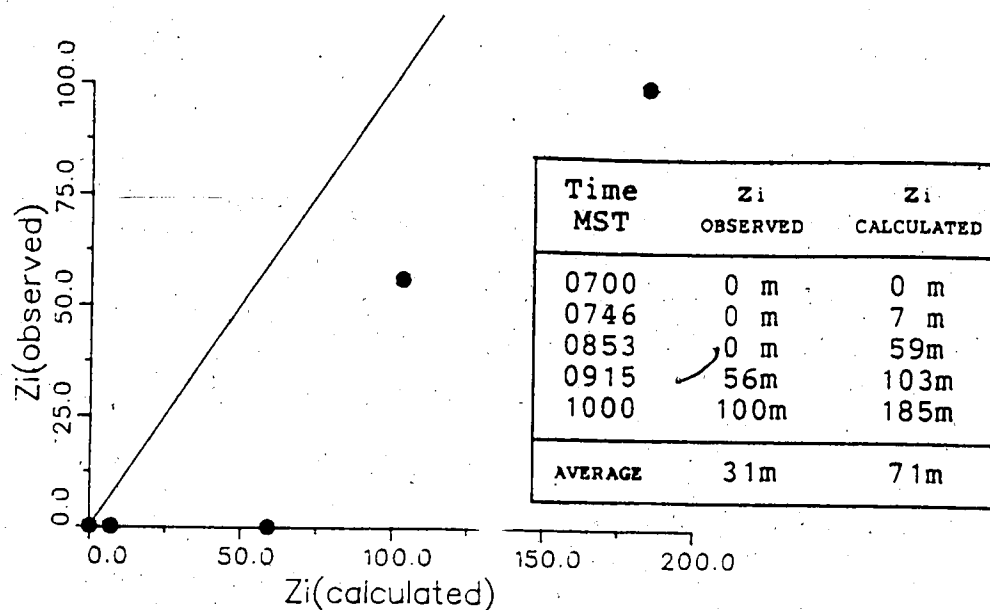


Fig. 4.21 Observed vs. calculated mixing heights with the encroachment model valid for October 12, 1987

On October 12, 1987 the encroachment model overestimated the observed mixing heights. However, the discrepancy appeared to increase with time at a much smaller rate of growth. We could even interpret this growth as negligible, in the average, by viewing the diagram.

On November 22, 1974 the GSE model (Fig. 4.22) overestimated the observed mixing heights and the discrepancy increased with time. This discrepancy appeared to be greater than the one characterizing the encroachment model.

On November 23, 1974 the same pattern was observed. The GSE model overestimated the observed mixing heights with an increasing discrepancy with time. However this discrepancy appeared to be smaller than that observed with the

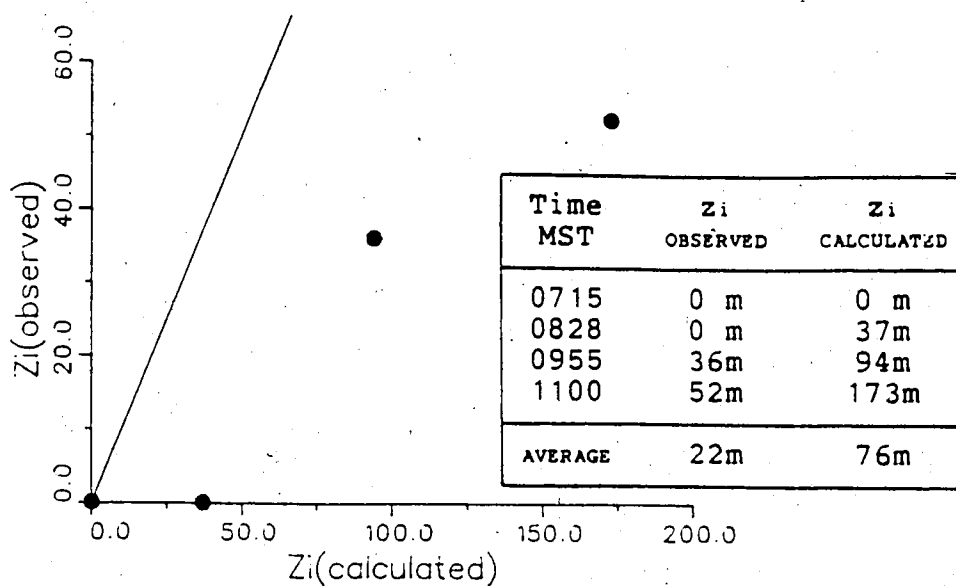


Fig. 4.22 Observed vs. calculated mixing heights with the G.S.E.-s.s. model valid for November 22, 1974

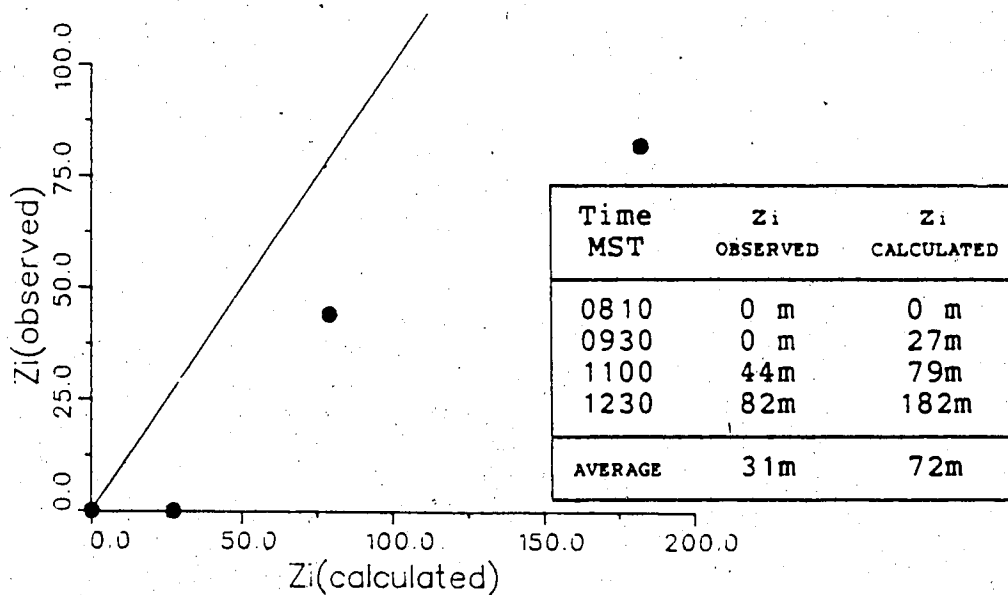


Fig. 4.23 Observed vs. calculated mixing heights with the G.S.E.-s.s. model valid for November 23, 1974

encroachment model.

On November 27, 1974 the GSE model appeared to make good low mixing height estimates, much better than the estimates made by the encroachment model. However the highest observed mixing height was underestimated and its discrepancy was greater than that found with the encroachment model.

On October 2, 1987 the GSE model overestimated the observed heights and the discrepancy increased with time. However this discrepancy was kept smaller than that found with the encroachment model.

On October 3, 1987 we observe a good estimate of the observed mixing heights made with the GSE model. Although the model overestimated the observed mixing heights the

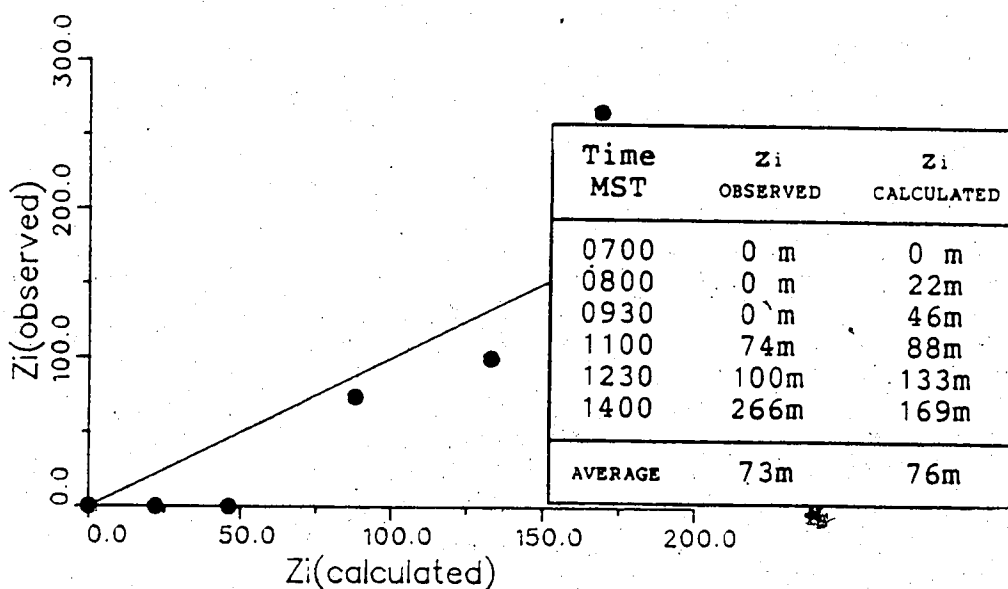


Fig. 4.24. Observed vs. calculated mixing heights with the G.S.E.-s.s. model valid for November 27, 1974.

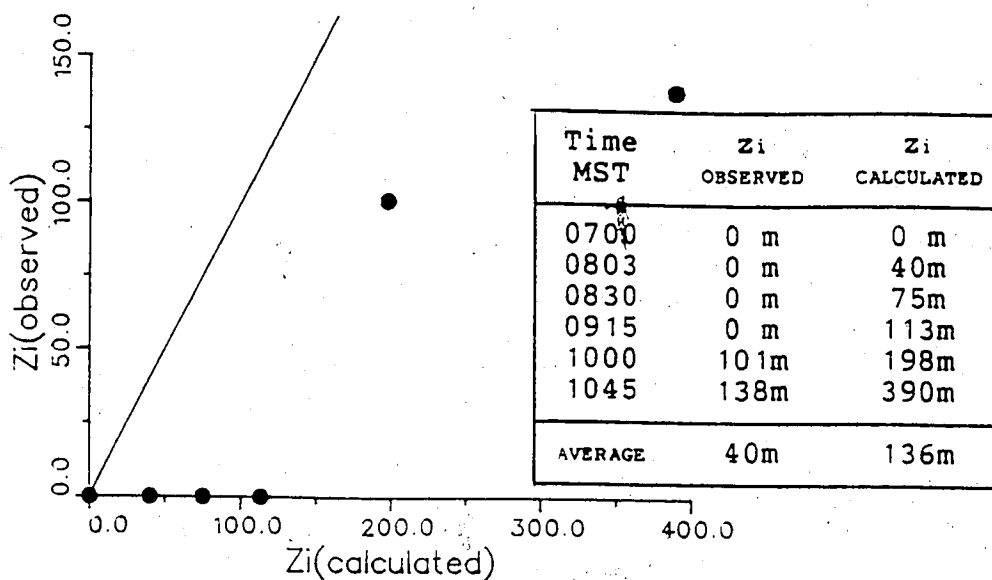


Fig. 4.25 Observed vs. calculated mixing heights with the G.S.E.-s.s. model valid for October 2, 1987

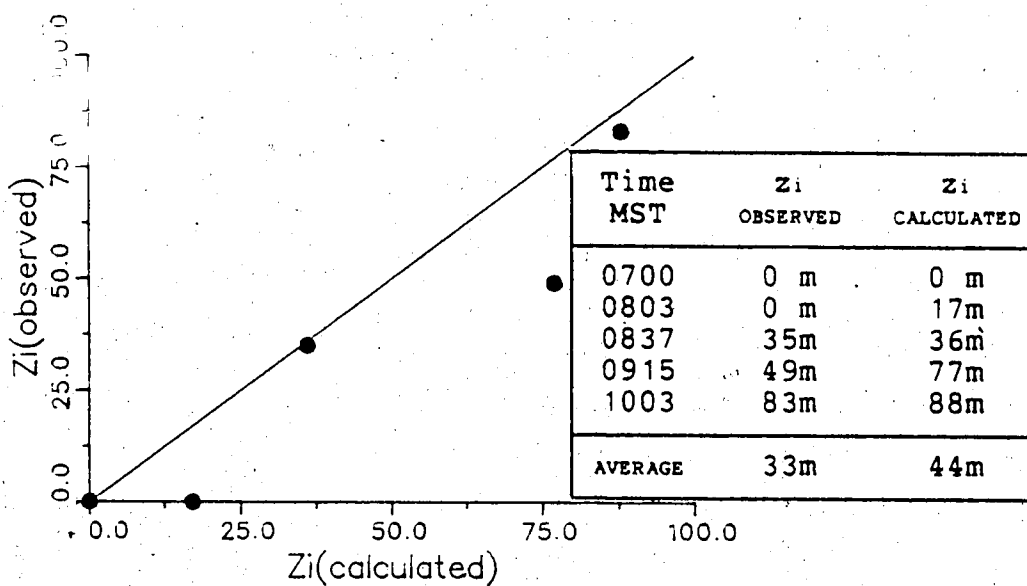


Fig. 4.26 Observed vs. calculated mixing heights with the G.S.E.-s.s. model valid for October 3, 1987

discrepancy was very small. In fact the estimated mixing height was 33% higher than the observed, compared to 66% higher with the encroachment model.

On October 6, 1987 the GSE model underestimated the observed mixing heights as a result of the cool air advection.

On October 12, 1987 the GSE model overestimated the observed mixing heights. However the discrepancy appeared to increase with time but with a growth rate smaller in magnitude compared with the encroachment model.

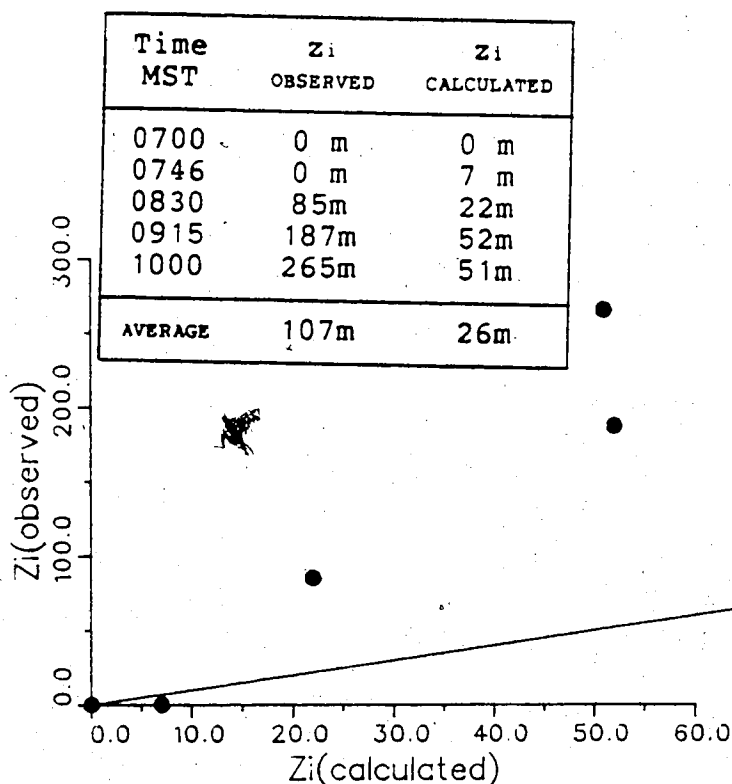


Fig. 4.27 Observed vs. calculated mixing heights with the G.S.E.-s.s. model valid for October 6, 1987

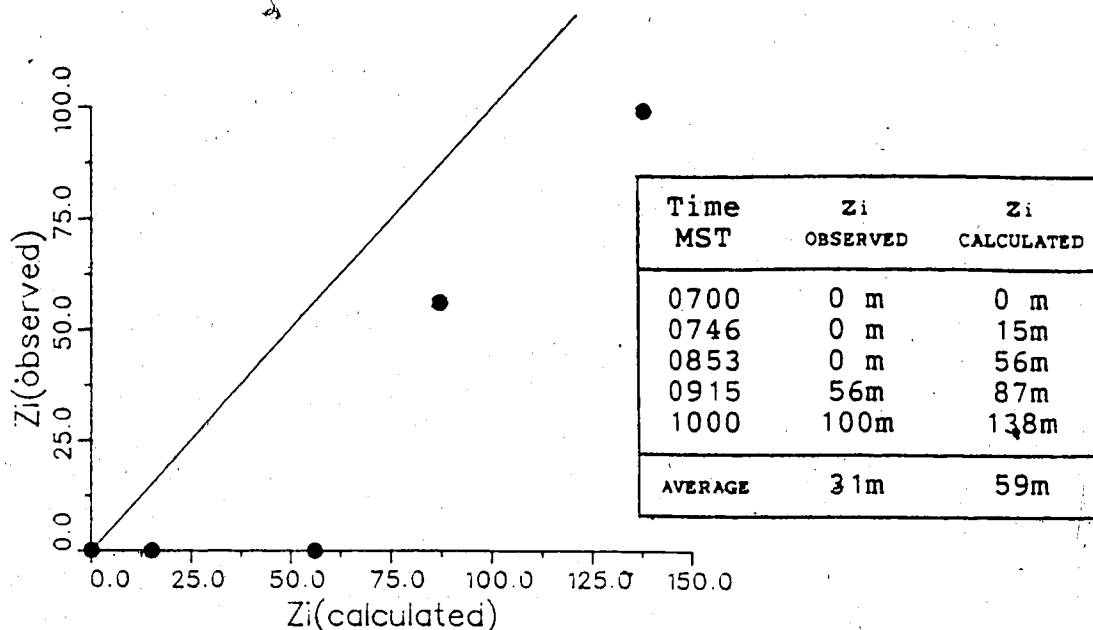


Fig. 4.28 Observed vs. calculated mixing heights with the G.S.E.-s.s. model valid for October 12, 1987

4.6 Estimation of the nocturnal inversion height and RMSE of the models.

There are actually three suggested ways to determine the nocturnal inversion height h_i at the time of minimum surface temperature:

a) From the temperature profile corresponding to the minimum surface temperature or for any practical purpose from the upper air weather stations information valid at 1200Z. Of course spatial differences always may incorporate an error, or

b) From the formula $h_i = 2(K_R \Delta t)^{1/2}$ where Δt is the time between the maximum temperature of the previous day and the minimum temperature of the current day. In this case we need also to

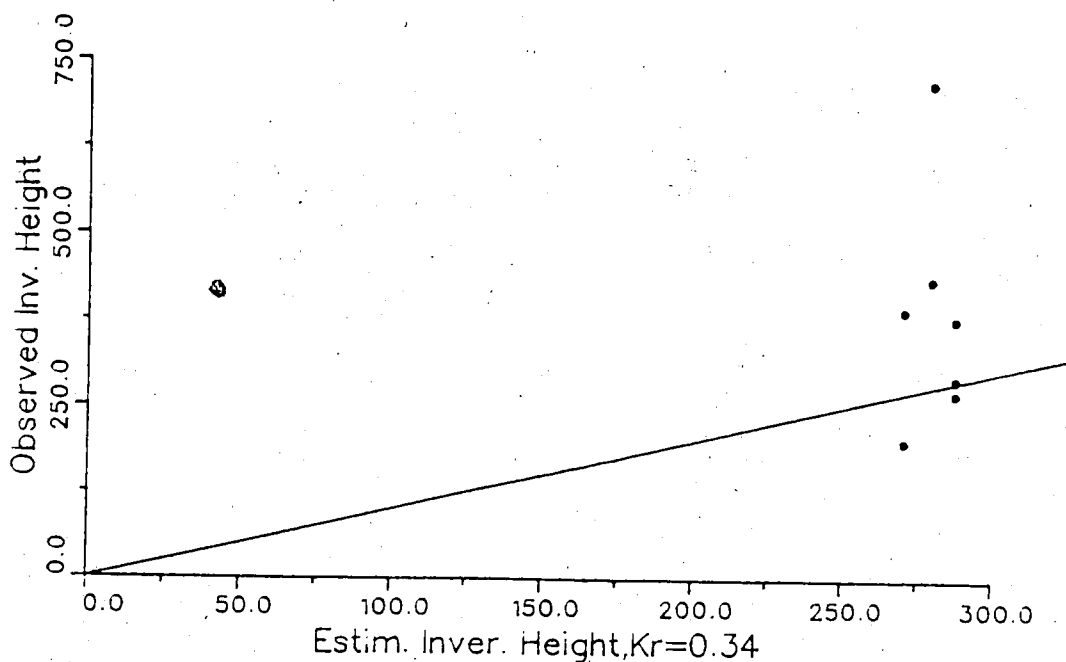


Fig. 4.29 Observed vs. estimated inversion height with $K_R=0.34\text{m}^2/\text{sec}$

evaluate the radiative diffusivity K_R . Anfossi et al (1976) suggest a value of $0.34\text{m}^2\text{s}^{-1}$. The author, based on the collected data from Ellerslie, derived a value of $0.11\text{m}^2\text{s}^{-1}$, and

c) From Anfossi's assumption that

$$T(h_i, t) - T_{\min}(0, t) \approx \lambda [T(0, 0) - T_{\min}(0, t)]$$

with λ lying in the range 0.5-0.65. Table 4.2 shows values of h_i estimated by the above methods. Fig. 4.29 shows that the estimated nocturnal inversion height underestimated those observed from the temperature profiles. Fig. 4.30 displays the relation of h_i estimated with the method (b)

Table 4.2 Estimation of the nocturnal inversion height

Date of experiment	h_i (profile)	h_i		h_i T(h_i, t)
		$K_R=0.34$	$K_R=0.11$	
74-11-22	720m	280m	170m	82m
74-11-23	291m	288m	175m	132m
74-11-27	378m	288m	175m	136m
87-10-02	390m	271m	164m	125m
87-10-03	270m	288m	175m	N/A
87-10-06	200m	271m	164m	N/A
87-10-12	435m	280m	170m	180m

and $K_R=0.11\text{m}^2\text{s}^{-1}$ and with the method (c). Although both (b) and (c) underestimate even more the observed inversion heights, they appear more comparable one with the other.

Tables 4.3 and 4.4 present the calculated root mean square error for the two models,

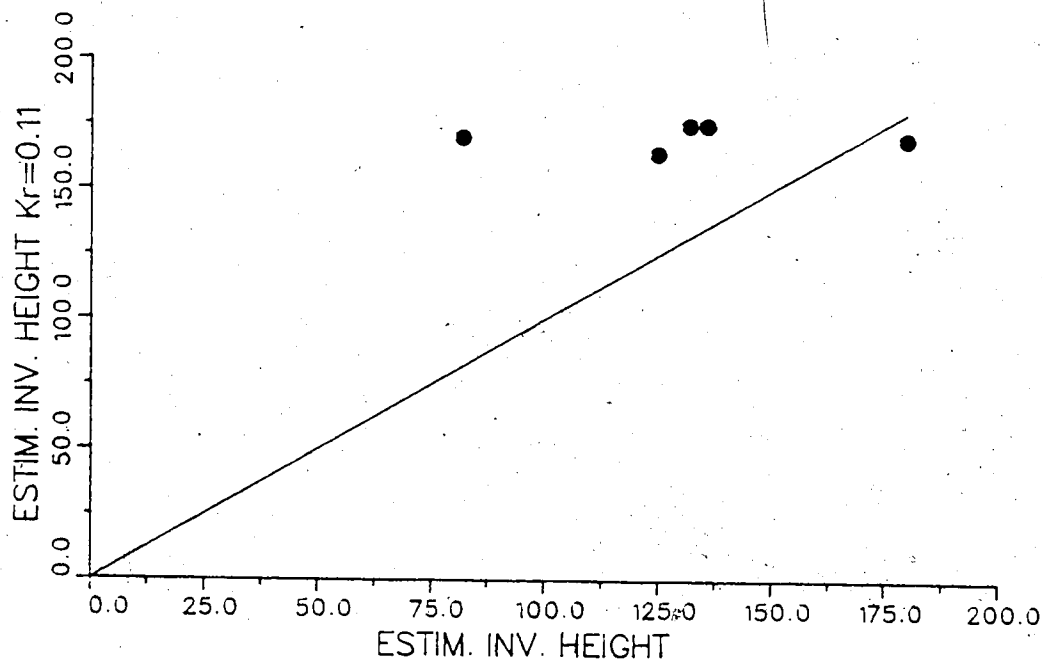


Fig. 4.30 Relation between estimated inversion heights with the methods (b) $K_R=0.11\text{m}^2/\text{sec}$ and (c)

$$A = \sum (\Delta z_i)^2, \quad B = (\sum (\Delta z_i)^2) / N, \quad C = [(\sum (\Delta z_i)^2) / N]^{1/2}$$

The overall RMSE for the encroachment model was 88m whereas for the GSE model it was 78m. The combined RMSE for the complete set of the estimated mixing heights by the models is 83m.

It appears therefore that the GSE-s.s. model had the smallest average error. With respect to the average observed mixing height of 48m both models appear to behave poorly. Garrett (1981) in his model makes the argument that an initial mixed-layer height of 50m is assumed as a starting height whereas he refers to the literature pointing out that the initial height is difficult to be standardized and defined precisely. Its value may be varied by 100m or more. Under this constraint he tested his model with observed data from four U.S. radiosonde stations for 1978. His annual RMSE was 41% of the mean observed mixing heights. In addition he excluded cases with maximum mixing heights <400m. In this model the observed mixing height has been determined as the intersection of the environment with a dry adiabat drawn from a 30m height. That was an attempt to minimize the effect of the superadiabatic surface layer. However no attempt was made to consider an initial mixed-layer height. Two more methods were exploited to determine the observed mixing height. These were the capping inversion and the "kink" method. With the capping inversion method the observed mixing height was determined at the point where an inversion of the potential temperature starts to develop.

Table 4.3 Estimation of the RMSE for the encroachment model

Date	Average Observed mixing height	Average Calculated mixing height	$\Delta z_i = z_i(\text{observed}) - z_i(\text{calculated})$						RMSE		
			1	2	3	4	5	6	A	B	C
74-11-22	22	74	0	-19	-52	-136	N/A	N/A	21201	5300.25	73m
74-11-23	31	98	0	-28	-59	-178	N/A	N/A	35949	8987.25	95m
74-11-27	73	95	0	-16	-45	-30	-73	36	9806	1634.33	40m
87-11-02	40	157	0	-38	-85	-148	-187	-252	127591	21265.17	146m
87-11-03	33	55	0	-15	-3	-53	-39	N/A	4564	912.8	30m
87-11-06	107	32	0	-3	63	120	199	N/A	57979	11595.80	108m
87-11-12	31	71	0	-7	-59	-47	-85	N/A	12964	2592.80	51m

Table 4.4 Estimation of the RMSE for the GSE-s.s. model

Date	Average Observed mixing height	Average Calculated mixing height	$\Delta z_i = z_i(\text{observed}) - z_i(\text{calculated})$						RMSE		
			1	2	3	4	5	6	A	B	C
74-11-22	22	76	0	-37	-58	-121	N/A	N/A	19374	4843.5	70m
74-11-23	31	72	0	-27	-35	-100	N/A	N/A	11954	2988.5	55m
74-11-27	73	76	0	-22	-46	-14	-33	97	13294	2215.67	47m
87-11-02	40	136	0	-40	-75	-113	-97	-253	93412	15568.67	125m
87-11-03	33	44	0	-17	-1	-28	-5	N/A	1099	219.8	15m
87-11-06	107	26	0	-7	63	135	214	N/A	68039	13607.80	117m
87-11-12	31	59	0	-15	-56	-31	-38	N/A	5766	1153.2	34m

With the "kink" method the mixing height was determined up to the point where a "significant" stable layer is established (Myrick, 1987). By "significant" stable layer is meant the layer with a potential gradient greater than $0.5\text{deg}/100\text{m}$ by at least $0.2\text{deg}/100\text{m}$. The Holzworth method described in Chapter 1 was used, where it was feasible, to determine the morning and afternoon mixing heights. Table 4.5 demonstrates a good correlation between the capping inversion method, the "kink" method and the "30m dry adiabat" method I used.

Table 4.5 Average observed mixing heights estimated by the indicated methods

Date	Holzworth method	Capping inversion	Kink method	30m Dry adiabat	Encroachment	GSE-s.s.
74-11-22	N/A	30m	19m	22m	74m	76m
74-11-23	N/A	66m	31m	31m	98m	72m
74-11-27	N/A	120m	47m	73m	95m	76m
87-10-02	45-315	18m	18m	40m	157m	136m
87-10-03	N/A-135	33m	28m	33m	55m	44m
87-10-06	160-2142	87m	58m	107m	32m	26m
87-10-12	N/A-90	27m	27m	31m	71m	59m

If we attempt to consider only mixing heights greater than 50m, and if we exclude data collected on October 6, 1987 when strong thermal advection occurred, we get an overall average of the observed mixing heights of 100m and an RMSE of 100m for the GSE-s.s. model (124m for the encroachment). Given that Anfossi's analytical solution gave good results up to heights of the order of 120m, we may expect the discrepancy

to increase noticeably above that height, something that the figures demonstrated.

5. Summary, Conclusions and Recommendations

Recent progress in the formulation of entrainment models for the morning erosion of nocturnal radiation inversions coupled with recent experimental support for Brunt's simplified model for the temperature profile in a nocturnal radiation inversion, led the author to try to combine these ideas into a model for the height of the mixed layer.

The model is applicable only after the time of minimum surface temperatures on mornings with well developed surface-based inversions. The model assumes that the inversion is purely the result of radiative heat loss from the earth's surface. In other words it was assumed that the skies were clear and that winds were light with no thermal advection. The analytical expression of Anfossi et al (1976) for the nocturnal temperature profile was used to describe the temperature profile of the stable layer during the onset of the convective activity.

Two simple models were employed:

1. The 'ENCROACHMENT' model, assuming no capping inversion ($\Delta\theta=0$).
2. The 'STEADY STATE GENERAL STRUCTURE ENTRAINMENT' model, assuming $\Delta\theta \neq 0$, $\Delta h \neq 0$ but constant.

Input for the models included the temperature difference between the maximum of the previous day and the morning minimum, current screen height temperatures during the day and the height of the nocturnal inversion the

time of the minimum temperature. To evaluate the effectiveness of the models, we conducted a series of experiments. The temperature profiles of the lowest 1km were recorded by releasing minisondes into the atmosphere every 45 min. A sonic anemometer installed at 10m height failed to provide reliable data of the turbulent heat fluxes over the period of the experiments. The interface between the theodolite B (see Fig. 3.1) and the computer failed after the first experimental day and forced us to assume an average rate of rise of the minisonde of 3m/s, in order to determine the heights on the temperature records. The experiments lasted four days in early October from 0600MST to 1100MST. Efforts were made to comply with weather conditions comparable to those assumed by the theory, not always successfully.

Other supporting measurements were wind data at 10m height, relative humidity, wet bulb temperature and net and incoming radiation.

The data used were the relative temperatures and the inversion heights. The program estimating the mixing heights was very simple and employed the iteration method. Every mixing height was calculated starting from the initial minimum temperature and not based on the estimated mixing height during the previous release. The program halts the mixed layer growth when the inversion height is reached. Both models provided similar results. Both tended to overestimate the observed mixing heights. However, a

tendency to underestimate the observed mixing heights was found when cool air advection occurred. The similarity of the results, that is overestimates and increased discrepancy with time, may be explained by the fact that the two expressions are reduced to one when the value of the parameter G is 1. G is the ratio of the lapse rates of the stable layer aloft to that of the entrainment layer. Attempts were made to determine G from the temperature profiles. They indicated that G may become as small as 0.1 (sometimes even smaller), depending on the time and the lapse rate of the nocturnal inversion. However, the steady state model for $G < 0.6$ implies a negative entrainment height Δh that cannot be justified. The model also appeared to be sensitive to the nocturnal inversion height which was one of the poorly calculated quantities. Ambiguities as to the appropriate radiative diffusivity and the weather conditions overnight existed. A very poor relation between the observed inversion height and that calculated by method (b) existed. The 1200Z radiosonde indicated lower inversion heights comparable to the ones calculated by methods (c) and (b) with a low value of K_R . The model appeared to be sensitive also to the temperature differences. Even the appearance of early morning frost may cause consumption of energy for evaporation and consequent delay of the mixing height growth. As a result the mixing heights would be overestimated.

Some possible reasons for the model's discrepancies are

summarized below:

1. Hour of observation. Early morning observations on October indicated that no mixing layer had developed. This also was confirmed with data taken by Alberta Environment from fall 1977 to fall 1983 (Myrick, 1987). This is because solar radiation cannot provide adequate heat at this hour of the day. Summer periods characterized by high temperatures and significant heat fluxes, should be more representative for our model.

2. Accuracy of temperature differences. In situ measurements of maximum and minimum temperature and their time of occurrence are needed. These differences enter in the model as independent variables to determine the mixing and the inversion heights. The model incorporates the ratio of the temperature difference and the inversion height. Given that the temperature difference is of the order of 10 and the inversion height of the order of 100 it should not underestimate the importance of its accuracy because the other terms of the analytical expression are equally small. The current temperature measurement at the surface is most likely to be higher than the mean potential temperature of the mixed layer due to the development of the superadiabatic surface layer. Therefore the current surface temperature should contribute to the overestimate of the observed mixing height.

3. The G factor. The steady state model is of limited use. The ratio of the lapse rates in the stable and the

entrainment layer should be reflected more realistically. When the actual G value is small, i.e. a relatively strong lapse rate is present in the entrainment layer, the mixing height growth should be slow since large turbulent heat fluxes from below are needed for effective mixing given that the heat flux from aloft is relatively weak. When G is large the mixing height growth should be faster since the stable layer entrains more heat in the mixed layer and more effective mixing is accomplished. Then if we assume G greater than the actual, an overestimate of the mixing height occurs.

4. Inversion height. The inversion height is another factor for which the model is sensitive. The relation between the mixing height and the inversion height is not obvious from the analytical expression, which appears to be rather complicated. A change of the inversion height with time may have therefore positive or negative results. The fact that the inversion heights that were used were much larger than those estimated by the other methods and the fact that the models overestimated the observed mixing heights leads to the opinion that higher inversion heights enhance the discrepancy between observed and estimated mixing heights. An increase of the inversion height with time may provide better estimates for large mixing heights. Appropriate care should be taken to ensure that the inversion height is the result of radiational cooling with no remaining inversions from previous nights or from thermal advection.

The conclusions of this study are as follows:

- (i) The minisonde is an excellent measuring system for this problem.
- (ii) Temperatures can be directly applied to mixed height estimations. In situ measurements of the maximum and minimum temperatures should be accurately recorded as well as the weather conditions overnight.
- (iii) The model is in its initial stage and needs refinement. However, it is very practical and may be used for quick estimates.
- (iv) Given that Garrett (1981) has excluded observed mixing heights <400m from his tests "to remove marginal growth days from the analysis" leads me to the conclusion that the errors of this model are reasonable and the model may be more accurate in low heights which are important for trapping of pollutants.
- (v) The General Structure Entrainment (steady state) model is more versatile and can be improved for more accurate estimates.
- (vi) It is often very difficult to identify $\Delta\theta$ or Δh with confidence from the observed temperature profiles. The very large temperature gradients in the lower part of the inversions are sensitive to small temperature-height errors.

Factors addressed previously need to be understood for accurate mixing height estimations. Suggested future work to answer some of the problems encountered in this study are summarized below:

1. Inversion height. As mentioned previously the inversion height is very poorly estimated. The relation of the observed inversion heights and the estimated should be established as accurately as possible. Possible additional variables may be needed, e.g. vapor pressure.

2. Entrainment effects. The entrainment process has been discussed by numerous authors as a factor which affects mixing heights. The entrainment layer may represent up to 20% of the mixed-layer height. The unsteady-state General Structure Entrainment model should be explored for better estimates of mixing heights.

3. Temperature difference. Anfossi's assumption $T_{\max} - T_{\min} = \frac{R_N}{K_R \rho_a c_p (1 - \text{erfc}(1))} \cdot \frac{h_i}{\sqrt{\pi}}$ needs to be explored. Anfossi claimed inability to verify this relation as a result of lack of data. An attempt to verify this relation by using overnight net radiation values in the present study revealed discrepancies.

4. Surface temperature error. Systematic errors incorporated in the mixing height due to higher surface temperatures in the superadiabatic layer may contribute in inaccuracies of the model.

Bibliography

- Anfossi D., P. Bacci, A. Longetto (1976) Forecasting of vertical temperature profiles in the atmosphere during nocturnal radiational inversions from air temperature trend at screen height, Quart. J. R. Met. Soc. 102: 173-180.
- Aron R. (1983) Mixing height-an inconsistent indicator of potential air pollution concentrations, Atmospheric Environment 17: 2193-2197.
- Ball F.K. (1960) Control of inversion height by surface heating, Quart. J. R. Met. Soc. 86: 483-494.
- Betts A.K. (1973) Non-precipitating cumulus convection and its parameterization, Quart. J. R. Met. Soc. 99: 178-196.
- Briggs G.A. (1969) Plume rise, U.S. Atomic Energy Commission, Critical Review Series, TID-25075, U.S. Department of Commerce, 81pp.
- Brunt D. (1939) Physical and Dynamical Meteorology, Cambridge at the University Press, 428pp.
- Brutsaert W. (1972) Radiation, evaporation and the maintenance of turbulence under stable conditions in the lower atmosphere, Boundary-Layer Meteorology 2: 309-325
- Businger J.A. (1972) Remote Sensing of the Troposphere, ch.6, Editor V.E. Derr, U.S. Government Printing Office, Washington, D.C.
- Carlslaw S.H. and J.C. Jaeger (1971) Conduction in Solids, 2nd Edition, Oxford at the Clarendon Press, 510pp.
- Carson D.J. (1973) The development of a dry inversion-capped convectively unstable boundary layer, Quart. J. R. Met. Soc. 99: 450-467.
- Carson D.J., F.B. Smith (1974) Thermodynamic model for the development of a convectively unstable boundary layer, Advances in Geophysics 18A: 111-124.
- Chorley L.G., S.J. Caughey, C.J. Readings (1975) The development of the Atmospheric boundary layer: 3 case studies, Met. Magazine 104: 349-360.
- Cleese B.A., S.J. Caughey, D.T. Tribble (1977) Information on the thermal structure of the Atmospheric Boundary

- Layer from acoustic sounding, Met. Magazine 106: 42-52.
- Deardorff J.W. (1967) Empirical dependence of the eddy coefficient of heat upon stability above the lowest 50m, J.A.M. 6: 631-643.
- Deardorff J.W. (1972b) Numerical investigation of neutral and unstable planetary boundary layers, J.A.S. 29: 91-115.
- Deardorff J.W., G.E. Willis, D.K. Lilly (1974) Comment on the paper by A.K. Betts "non-precipitating cumulus convection and its parameterization", Q.J.R.M.S. 100: 122-123.
- Deardorff J.W. (1976) On the entrainment rate of a stratocumulus topped mixed layer, Q.J.R.M.S. 102: 563-582.
- Deardorff J.W. (1979) Prediction of convective mixed layer entrainment for realistic capping inversion structure, J.A.S. 36: 424-436.
- Deardorff J.W. (1980) Progress in understanding entrainment at the top of a mixed layer, Workshop on the Planetary Boundary Layer, Proceedings of workshop on the Planetary Boundary Layer, 14-18 Aug., 1978, American Meteorological Society.
- Dobbins R. (1979) Atmospheric Motion and Air Pollution, J. Wiley & Son Inc., 323pp.
- Elliot W.P. (1964) The height variation of vertical heat flux near the ground, Q.J.R.M.S., 90: 260-265.
- Environment Canada Monthly Record, Meteorological Observations in Canada, November 1974.
- Garnett A.J. (1981) Comparison of observed mixed layer depths to model estimates using observed temperatures and winds, and MOS Forecasts, J.A.M. 20: 1277-1283
- Hanna S.R., G.A. Briggs, J.W. Deardorff, B.A. Egan, F.A. Gifford, F. Pasquill (1977) AMS Workshop on Stability Classification Schemes and σ curves, Bul. of A.M.S. 58: 1305-1309.
- Hanna S.R., C.L. Burkhardt, R.J. Paine (1980) Mixing height uncertainties, Workshop on the Planetary Boundary Layer, 14-18 August 1978, American Meteorological Society.
- Hanna S.R., G.A. Briggs, R.P. Hosker, Jr. (1982) Handbook of Atmospheric Diffusion, U.S. Department of Energy, 102pp.

- Hildebrand P.H., B. Ackerman (1984) Urban effects on the convective boundary layer, J.A.S. 41: 76-91
- Holzworth G.C. (1967) Mixing depths, wind speeds and Air Pollution for selected locations in the United States, J.A.M. 6: 1039-1044.
- Holzworth G.C. (1971) Meteorological Potential for Urban Air Pollution in the Contiguous U.S., in the Proceedings of the 2nd International Clean Air Congress, H.M. England and W.T. Berry, Editors, Academic Press, New York.
- Holzworth G.C. (1972) Mixing Heights, Wind speeds and potential for Urban Air pollution throughout the contiguous United States, Office of Air Programs, Publication No AP-101, Environmental protection Agency, Research Triangle Park, N.C.
- Houghton T. J. (1980) The Physics of Atmospheres, Cambridge University Press, 271pp.
- Ingersoll L.R., O.J. Zebel, A.C. Ingersoll (1948) Heat conduction with Engineering and Geological Applications, Mc Graw Hill, New York, 278pp.
- Kaimal J.C., J.C. Wyngaard, D.A. Haugen, O.R. Cote, Y. Izumi (1976) Turbulence structure in the convective boundary layer, J.A.S. 33: 2152-2169.
- Lenschow D.H. (1970) Airplane measurements of planetary layer structures, J.A.M. 9: 874-884.
- Lilly D.K. (1968) Models of cloud-topped mixed layers under a strong inversion, Q.J.R.M.S. 94: 292-309.
- Mc Bean G.A. (1979) The Planetary Boundary Layer, WMO Technical Note 165, WMO-No 530, Secretariat of the World Meteorological Organization, Geneva, Switzerland.
- Moulsley T.J., D.N. Asimakopoulous, R.S. Cole, B.A. Crease, S.J. Caughey (1981) Measurement of boundary layer structure parameter profiles by acoustic sounding and comparison with direct measurements, Q.J.R.M.S. 107: 203-230.
- Myrick R. (1987) Mixing height Climatology of Edmonton, Alberta, Internal Memorandum, Alberta Environment.
- Nieuwstadt F.T.M., H. van Dop (1980) (Editors) Atmospheric Turbulence and Air pollution Modelling, D. Reidel Publishing Co., Holland, 358pp.
- Nieuwstadt F.T.M., H. Tennekes (1981) A rate equation for the nocturnal boundary layer height,

- J.A.S. 38: 1418-1428.
- Nieuwstadt F.T.M., (1984) Some aspects of the turbulent stable boundary layer, *Boundary Layer Meteorology* 30: 31-55.
- Olson R. (1985) The climate of Edmonton, *Climatological Studies #37, The Climate of Canadian Cities #2*, Canadian Publishing Center, Supply and Services, Ottawa, Canada, Cat# En 57-7/37E.
- Pasquill F., F.B. Smith (1983) *Atmospheric Diffusion*, 3rd edition 437pp., Ellis Horwood Ltd.
- Plate E.J. (1971) Aerodynamic characteristics of atmospheric boundary layers, *Critical Review Series, TID 25465*, U.S. Atomic Energy Commission, U.S. Department of Commerce, 198pp.
- Plate E.J. (1982) (Editor) *Engineering Meteorology*, Elsevier Scientific Publishing Co, 740pp.
- Portelli R.V. (1977) Mixing heights, wind speeds and ventilation coefficients for Canada. *Atmospheric Environment Service, Climatological Studies #31*
- Reddick H.W., F.H. Miller (1948) *Advanced Mathematics for Engineers*, John Wiley & Son Inc., 508pp.
- Richter J.H., D.R. Jensen, V.R. Noonkester, T.G. Konrad, A. Arnold, J.R. Rowland (1974) Clear Air Convection: A close look at its evolution and structures, *Geophysical Research Letters* 1-2: 173-176.
- Sun Wen Yih, Chiao-Zien Chang (1986) Diffusion model for a convective layer. Part II: Plume released from a continuous point source, *J. of Climate and Applied Meteorology* 25: 1454-1463.
- Sutton O.G. (1953) *Micrometeorology*, Mc Graw Hill Co., Inc., London, 333pp.
- Trenberth K.E., G.M. Driendonks (1980) Basic Entrainment equations for the atmospheric boundary layer, *Boundary Layer Meteorology* 20: 515-527.
- Tennekes H., J.L. Lumley (1972) *A First course in Turbulence*, M.I.T. Press, Cambridge, Mass., 300pp.
- Turner J.S. (1973) *Buoyancy effects in fluids*, Cambridge University Press, 367pp.
- Whitaker S. (1975) *Elementary Heat Transfer Analysis*, Pergamon Press Inc., U.S.A., 369pp.

Zdunkowski W.G., F.G. Johnson (1965) Infrared flux
divergence calculations with newly constructed radiation
tables, J.A.M. 4: 371-377.

Appendix I

```

C THIS PROGRAM COMPUTES THE MIXING HEIGHT DURING THE ENCR-
C ACHMENT STAGE. THE NOCTURNAL INVERSION HEIGHT IS ESTIMA-
C TED FROM THE TAYLOR'S FORMULA BY REPLACING THE DIFFUSI-
C VITY BY THE RADIATIONAL DIFFUSIVITY. THE INITIAL NOCTUR-
C NAL HEIGHT IS ESTIMATED FROM THE FIRST MINISONDE RELEASE
C BEFORE SUNRISE. THIS FORMULA INVOLVES THE TIME AT WHICH
C THE MINIMUM TEMPERATURE WAS REACHED  $t_{min}$ .:
C  $NIH = \sqrt{4 * KR * (t - t_{min})}$ ; t IS THE CURRENT TIME OF TAKING
C THE SURFACE TEMPERATURE.
C N IS THE NUMBER OF DAYS.
C M IS THE NUMBER OF SURFACE TEMPERATURES TAKEN AT DIFFERENT
C TIMES t, WITH THETAO(I) BEING THE FIRST SURFACE TEMPERATURE
C MEASURED AND THETAM(I,J) ALL THE SURFACE TEMPERATURES.
C THETAO(I) INCLUDED. THE THETAM(I,J) CORRESPOND TO THE
C AVERAGE TEMPERATURES OF THE MIXING LAYER WHEN THAT IS DE-
C VELOPPED DURING THE MORNING HOURS.
C THE MIXING HEIGHT IS DETERMINED BY ITERATION, FROM THE FOR-
C MULA OF THETA(I,J) AND ZMX(I,J).
C DELT(I) IS THE TEMPERATURE DIFFERENCE BETWEEN THE MAXIMUM
C TEMPERATURE OF THE PREVIOUS DAY AND THE MINIMUM OF THE CUR-
C RENT DAY.
C CP IS THE SPECIFIC HEAT OF DRY AIR 1004 JOULE/KILOG.DEGREE
C KR IS THE RADIATIONAL DIFFUSIVITY 1224 M2/HR. ACCORDING
C TO ANFOSSI, OR 450 M2/HR, ACCORDING TO ELLERSLIE'S EXPE-
C RIMENTAL DATA.
C DENSA IS THE AIR DENSITY: 1.14Kg/M3
C CONSTANTS AND ALL DIMENSIONAL VARIABLES ARE IN UNITS OF Kg.m.
C Hr, Deg.
C READ(5,*)N
C REAL NIH(7,6),KR,NIHO(7)
C DIMENSION THETAO(7),THETAM(7,6),DELT(7),DTH(7,6),THETAH(7,6),
C #ZS(7,6),ZMX(7,6),DT(4,6)
10 FORMAT(1X,I2)
C DZS=0.0001
C KR=450
C KR=1224
C KR=0
C DO 11 I=1,N
C READ(5,30)M,DELT(I),THETAO(I),NIHO(I)
30 FORMAT(1X,I1,1X,F4.1,1X,F5.1,1X,F5.1)
C DO 77 J=1,M
C READ(5,40)THETAM(I,J),DT(I,J)
40 FORMAT(1X,F5.1,1X,F4.1)
77 CONTINUE
C DO 22 J=1,M
C ZS(I,J)=0.0
C NIH(I,J)=NIHO(I)+SQRT(4*KR*DT(I,J))
C DTH(I,J)=(THETAM(I,J)-THETAO(I))/NIH(I,J)
111 THETAH(I,J)=0.0098*ZS(I,J)-(DELT(I)/NIH(I,J))*
C *(EXP(-ZS(I,J)*ZS(I,J))-1.7725*ZS(I,J)*ERFC(ZS(I,J)))+
C #0.278*ZS(I,J)-1)
C IF(THETAH(I,J).GE.DTH(I,J))GO TO 15
C IF(ZS(I,J).GE.1.0)GO TO 15
C ZS(I,J)=ZS(I,J)+DZS
C GO TO 111
15 ZMX(I,J)=ZS(I,J)*NIH(I,J)
22 CONTINUE
C DO 44 J=1,M
C WRITE(4,20)I,J,ZMX(I,J),I,J,THETAH(I,J),I,J,DTH(I,J)
20 FORMAT(' ',ZMX(' ',I1,' ',I1,' ')=' ',F8.4,' ',THETAH(' ',I1,' ',I1,
C #')=' ',F8.4,' ',DTH(' ',I1,' ',I1,' ')=' ',F8.4)
44 CONTINUE
11 CONTINUE
C STOP
C END

```

Appendix II

```

C   THIS PROGRAM COMPUTES THE MIXING HEIGHT DURING THE EN-
C   TRAINMENT STAGE UNDER STADY STATE CONDITIONS.
C   THE NOCTURNAL INVERSION HEIGHT IS ESTIMA-
C   TED FROM THE TAYLOR'S FORMULA BY REPLACING THE DIFFUSI-
C   VITY BY THE RADIATIONAL DIFFUSIVITY. THE INITIAL NOCTUR-
C   NAL HEIGHT IS ESTIMATED FROM THE FIRST MINISONDE RELEASE
C   BEFORE SUNRISE. THIS FORMULA INVOLVES THE TIME AT WHICH
C   THE MINIMUM TEMPERATURE WAS REACHED tmin.:
C   NIH=SQRT(4*KR*(t-tmin));t IS THE CURRENT TIME OF TAKING
C   THE SURFACE TEMPERATURE.
C   N IS THE NUMBER OF DAYS.
C   M IS THE NUMBER OF SURFACE TEMPERATURES TAKEN AT DIFFERENT
C   TIMES t, WITH THETAO(I) BEING THE FIRST SURFACE TEMPERATURE
C   MEASURED AND THETAM(I,J) ALL THE SURFACE TEMPERATURES.
C   THETAO(I) INCLUDED. THE THETAM(I,J) CORRESPOND TO THE
C   AVERAGE TEMPERATURES OF THE MIXING LAYER WHEN THAT IS DE-
C   VELOPPED DURING THE MORNING HOURS.
C   THE MIXING HEIGHT IS DETERMINED BY ITERATION, FROM THE FOR-
C   MULA OF THETA(I,J) AND ZMX(I,J).
C   DELT(I) IS THE TEMPERATURE DIFFERENCE BETWEEN THE MAXIMUM
C   TEMPERATURE OF THE PREVIOUS DAY AND THE MINIMUM OF THE CUR-
C   RENT DAY.
C   CP IS THE SPECIFIC HEAT OF DRY AIR 1004 JOULE/KILOG.DEGREE
C   KR IS THE RADIATIONAL DIFFUSIVITY 1224 M2/HR , ACCORDING
C   TO ANFOSSI, OR 450 M2/HR, ACCORDING TO ELLERSLIE'S EXPE-
C   RIMENTAL DATA.
C   DENSA IS THE AIR DENSITY: 1.14Kg/M3
C   CONSTANTS AND ALL DIMENSIONAL VARIABLES ARE IN UNITS OF Kg.m.
C   Hr. Deg.
      READ(5,10)N
      REAL NIH(7,6),KR,NIHO(7)
      DIMENSION THETAO(7),THETAM(7,6),DELT(7),DTH(7,6),THETAH(7,6),
      #ZS(7,6),ZMX(7,6),DT(7,6)
10  FORMAT(1X,I2)
C   G=0.20
C   G=0.40
C   G=0.60
C   G=0.80
C   G=0.85
C   G=0.90
C   G=0.98
C   G=1.00
C   G=1.20
C   G=1.40
      G=1.50
      Y=0.55*EXP(-0.27*G)
      YG=Y/(G+Y-1)
      GY=(1-G)/(G*(G+Y-1))
      PZS=0.0001
C   KR=450
C   KR=1224
      KR=0
      DO 11 I=1,N
      READ(5,30)M,DELT(I),THETAO(I),NIHO(I)
30  FORMAT(1X,I1,1X,F4.1,1X,F5.1,1X,F5.1)
      DO 77 J=1,M
      READ(5,40)THETAM(I,J),DT(I,J)
40  FORMAT(1X,F5.1,1X,F4.1)
77  CONTINUE
      DO 22 J=1,M

```

(cont'd)

```

ZS(I,J)=0.0
NIH(I,J)=NIHO(I)+SQRT(4*KR*DT(I,J))
DTH(I,J)=(THETAM(I,J)-THETAO(I))/NIH(I,J)
111 THETAH(I,J)=0.0098*(YG-GY)*ZS(I,J)-
#(DELT(I)/NIH(I,J))*(EXP(-(YG*ZS(I,J))**2)-1.7725*(YG-GY)*
#ZS(I,J)*ERFC(YG*ZS(I,J))+0.278*(YG-GY)*ZS(I,J)-1)
IF(THETAH(I,J).GE.DTH(I,J))GO TO 15
IF(ZS(I,J).GE.1.0)GO TO 15
ZS(I,J)=ZS(I,J)+DZS
GO TO 111
15 ZMX(I,J)=ZS(I,J)*NIH(I,J)
22 CONTINUE
DO 20 J=1,M
WRITE(4,20)I,J,ZMX(I,J),I,J,THETAH(I,J),I,J,DTH(I,J)
20 FORMAT(' ',I1,' ',I1,' ')=' ',F8.4,' ',THETAH(' ',I1,' ',I1,
#')=' ',F8.4,' ',DTH(' ',I1,' ',I1,' ')=' ',F8.4)
C WRITE(4,20)I,J,ZMX(I,J),THETA,DT
C 20 FORMAT(' ',I1,' ',I1,' ')=' ',F8.4,' ',THETA=' ',F8.4,
C #',DT=' ',F8.4)
44 CONTINUE
11 CONTINUE
STOP
END

```